Doctorate Dissertation

博士論文

Influence on deep-sea ferromanganese nodules and planktonic foraminifera by ocean acidification

（海洋酸性化における深海底鉄マンガンノジュールおよび浮遊性有孔虫への影響）

A Dissertation Submitted for Degree of Doctor of Philosophy

November 2018

平成 **30** 年 **11** 月博士（理学）申請

Department of Earth and Planetary Science, Graduate School of Science,

The University of Tokyo

東京大学大学院理学系研究科地球惑星科学専攻

Quan Wang

王 権

Abstract

Ocean acidification caused by increased atmospheric carbon dioxide (CO_2) will lead to enhanced acidity and lowered carbonate ion concentration in the marine environment. Most of the atmospheric CO_2 absorbed by the oceans resides in relatively shallow waters; however, surface seawaters are slowly mixing with the intermediate and deep seawaters of the oceans. Over time, this acidification effect will spread to the deep oceans. Due to the lack of carbonate as a natural buffer to pH decrease, the deep-sea environments are more vulnerable to pH changes. The response of metal-rich deep-sea ferromanganese (Fe–Mn) nodules to predicted pH values have been investigated in Chapter 2. On the other hand, marine organisms such as planktonic foraminifera build their shells by using the carbonate ion from the seawater, the influence of seawater chemistry changes on planktonic foraminifera, *Globigerinoides ruber* (white), have been discussed in Chapter 3.

The experiments by using phosphate buffer solutions revealed that the release of element from deep-sea Fe–Mn nodules is not simply increased in response to pH decrease. The element behavior is mainly regulated by sorption-desorption processes which are primarily determined by changes in the acidity of the solutions and ion species in the solutions. Based on this result, we improved the assessment by introducing artificial seawaters and a CO_2-induced pH regulation system. The pH changes caused by ocean acidification are simulated by adjusting the pH of the artificial seawaters through altering the partial pressure of CO_2. The improved

experiments revealed that the pH decrease caused by ocean acidification would promote the elements those exist as positively charged ions or complexes to release from the deep-sea sediments and restrain the elements those exist as negatively charged ions or complexes to be exchanged into the seawaters.

In order to investigate the response of the foraminiferal shells to ocean acidification, a piston core collected from above the lysocline in the East China Sea was used. The shells of planktonic foraminifera *Globigerinoides ruber* (white) were picked and performed weight/size measurements and X-ray microcomputed tomography (XMCT) measurements. The size-normalized weight of *Globigerinoides ruber* (white) covaries well with atmospheric pCO_2, which agrees with previous studies and manifest that the size-normalized weight of planktonic foraminiferal shells primarily reflects the changes of carbonate chemistry in surface seawaters. The high-resolution XMCT results helped to verify the post-depositional alteration and revealed that ocean acidification affects the shell volume (i.e., shell wall thickness) rather than shell density of planktonic foraminifera *G. ruber* (w).

Contents

Chapter 1

General Introduction

1. Carbon cycle, atmospheric CO_2, and ocean acidification

1.1. Carbon cycle and the oceans

Carbon is exchanging among the terrestrial biosphere, the oceans, the atmosphere, and the sediments through various chemical processes, which is known as the carbon cycle. (Falkowski et al. 2000; Raven et al. 2005). The oceans act as an important reservoir in the carbon cycle as carbon dioxide (CO_2) can be adsorbed into the seawaters and release back to the atmosphere. The transportation of CO_2 into the oceans occurs in two different processes, one is air-sea gas exchanges, and the other is biological uptake (Field et al. 1998; Falkowski et al. 2000).

The oceans act as a significant carbon reservoir and play an important role in the carbon sink. The oceans reserve about 3.8×10^4 Gt (gigatons; 1 Gt = 10^{15} grams) of carbon, which is more than 55 times of the atmosphere reservoir and 19 times of the terrestrial biosphere. The surface oceans adsorb 102 Gt of carbon per year meanwhile releasing about 100 Gt into the atmosphere. Comparing with the carbon exchanges between other reservoirs, the net sink of atmospheric carbon into the oceans is quite small. However, the oceanic uptake is a notable proportion compared to the total amount of anthropogenic carbon release (6 Gt per year) into the atmosphere (Raven et al. 2005).

The carbon in some reservoirs, such as rocks, sediments, and deep-sea water masses, hardly affect the carbon exchange in the surface oceans or the atmosphere on millennial timescales since carbon in these reservoirs exchanges on relatively longer geological

timescales. However, since the pre-industrial era, human activities have greatly accelerated the carbon exchange rate among these reservoirs and led to a dramatic increase in the concentration of atmospheric CO_2 (IPCC 2013).

1.2. Atmospheric CO_2 and ocean acidification

Atmospheric CO_2 levels increased from pre-industrial levels of approximately 280 ppmv (parts per million by volume) to nearly 410 ppmv (NOAA 2018). This increasing rate is at least an order of magnitude faster than has occurred for millions of years and is mainly driven by human fossil fuel combustion and deforestation (Doney and Schimel 2007; Doney et al. 2009). The atmospheric CO_2 would be approximately 450 ppmv today without being tempered by surface ocean uptake. The oceanic uptake processes account for nearly 30% of anthropogenic CO_2 added to the atmosphere (Sabine et al. 2004). Ocean uptake will help to moderate future climate change caused by increased atmospheric pCO_2; however, it is not harmless. The absorption of atmospheric CO_2 into seawater causes seawater acidity reductions and alterations in carbonate chemical balances. These processes are commonly referred to as ocean acidification. Absorption of atmospheric CO_2 into the oceans increased the seawater acidity, reduced pH, and lowered calcium carbonate saturation in surface seawaters (Caldeira and Wickett 2003, 2005; Feely et al. 2004; Orr et al. 2005; Feely et al. 2013).

2. Effects of Ocean Acidification and carbonate chemistry in seawater

2.1. The acidity and carbonate chemistry in the oceans

According to Henry's Law, an increase in the atmospheric level of CO_2 increases the concentration of CO_2 in the surface seawaters. CO_2 exists in the atmosphere as a chemically unreactive gas. However, once dissolved in seawater, it becomes reactive and takes part in a couple of geochemical processes. The reaction between CO_2 and water (H_2O) to form carbonic acid (H_2CO_3), and the decomposition of H_2CO_3 release carbonate ions (CO_3^{2-}) and hydrogen ions (H^+) into the seawater. Consequently, dissolution of CO_2 into the surface seawaters affects the acidity and carbonate chemistry of the oceans.

A series of geochemical processes across the ocean-atmosphere interaction surface governs the acidity and carbonate chemistry of the seawaters.

(1) $$CO_{2(atm)} \leftrightarrow CO_{2(aq)}$$

(2) $$CO_{2(aq)} + H_2O \leftrightarrow H_2CO_3$$

(3) $$H_2CO_3 \leftrightarrow H^+ + HCO_3^-$$

(4) $$HCO_3^- \leftrightarrow H^+ + CO_3^{2-}$$

Air-sea gas exchange equilibrates CO_2 concentration in the surface water to atmospheric levels within approximately one year, and the processes are reversible and near equilibrium (Millero et al. 2002). Once the atmospheric CO_2 adsorbed into seawater to form aqueous CO_2 (1), CO_2 reacts with water to form H_2CO_3 (2), which can then dissociate by releasing hydrogen ions to form bicarbonate ions (HCO_3^-) (3) and carbonate ions (CO_3^{2-}) (4).

Absorption of CO_2 into the seawater increases the concentrations of aqueous CO_2, HCO_3^-, and H^+; and in turn, lowers the pH of seawaters and concentration of CO_3^{2-}.

CO_2 dissolves into the seawaters and mainly exists as three inorganic forms: CO_2, HCO_3^-, and CO_3^{2-}. The sum of these three inorganic forms is known as dissolved inorganic carbon (DIC). The relative proportion of the three inorganic forms varies with the acidity of the seawater, and the amount of DIC changes according to the total alkalinity, temperature, and pressure of the seawaters. Under the current ocean condition, only about 1% of DIC is in the form of dissolved CO_2, and most of it is in the form of HCO_3^- (91%) and CO_3^{2-} (8%) (Raven et al. 2005).

2.2. pH variation in the oceans

The most direct effect of ocean acidification is the pH changes in the seawaters. The current surface oceans have an average pH of about 8.2, while this value can vary within ±0.3 units due to regional and seasonal factors. The spatial variation of the pH values of the oceans is primarily controlled by the surface temperature of the oceans and the upwelling of CO_2-rich deep water. Lower sea surface temperature enhances the dissolution of atmospheric CO_2 into the seawaters, while elevated seawater temperature reduces the amount of CO_2 in the oceans. When CO_2 dissolves into seawaters at a fixed temperature, the pH of the seawater decreases. In general, the water masses in the deep oceans have higher CO_2 concentration since organic materials exported from the surface biological production decompose and result

in CO_2 addition into the deep waters. When this CO_2-rich and low pH deep water upwells to the surface, it alters the pH distribution in the surface waters (Raven et al. 2005).

The temporal variation of seawater pH values in response to the changes in atmospheric CO_2 concentration can be theoretically estimated. Zeebe and Wolf-Gladrow (2001) predicted that the surface seawater pH would fall to below 7.9 by 2100. However, they just considered the surface ocean surfaces as a single "box" (constant sea surface temperature, salinity, and an initial pH of 8.2) without water masses mixing and assumed that anthropogenic release of CO_2 continues to be the current trend. Caldeira and Wickett (2003) performed a more detailed estimate using an ocean general-circulation model with observed pressure of atmospheric CO_2 from 1975 to 2000 and with CO_2 emission from the Intergovernmental Panel on Climate Change's IS92a scenario for 2000-2100. Their result showed that the initial changes of the seawater pH in the surface ocean are rapid and that the response of the deep is quite slow. However, as CO_2 continues to dissolve into the seawaters, the acidification effect is slowly transferred from the shallow to the deep oceans. With the continuous rise in CO_2 emissions from human activities, the pH of surface seawaters will potentially decline from 8.1 to 7.4, while the pH reduction of the deep-sea counterpart will be about 0.4 units, declining from about 7.6 to 7.2.

2.3 DIC as a pH buffer in the oceans

The DIC in seawater acts to buffer the changes of seawater acidity. HCO_3^- and CO_3^{2-},

the primary forms of DIC, are the major contributors to seawater alkalinity as well. The relative proportion of the three forms of DIC regulates the seawater acidity within a relatively narrow range. When additional hydrogen ions are added into the seawaters due to acidification processes (such as CO_2 adsorption), CO_3^{2-} reacts with the additional hydrogen ions and form HCO_3^-. This process diminishes the effect of acidification so that the pH drop is less than expected. However, this process also consumes some CO_3^{2-}; therefore, when an acid (such as CO_2 in the case of ocean acidification) is continually added into the seawaters, the buffer capacity of the seawaters to restrict pH changes declines.

On the other hand, the interaction of the deep waters with carbonate-rich sediments can compensate the pH buffer capacity of the oceans. On the longer timescales of ocean mixing, some carbonate fraction in the sediments dissolves into the seawater to compensate the concentration of CO_3^{2-}, so that changes in seawater acidity can be restricted further. However, this compensation effect greatly depends on the distribution of seafloor carbonate sediments. The pH buffer capacity is limited in the deep-sea area where carbonate sediments are rare.

2.4. Carbonate distribution in the oceans

Most carbonate ($CaCO_3$) is produced within the sea surface by marine organisms, such as foraminifera and coccolithophorid, and transported to deep oceans through “biological pump”. Only about 50% of the $CaCO_3$ exported from the surface to the deeper waters. In this portion, about 30% finally preserved in the sediments and less than 15% of the $CaCO_3$ is

dissolved throughout the water column (Archer 1996; Milliman and Droxler 1996).

The $CaCO_3$ production in the surface oceans combining with the $CaCO_3$ dissolution processes through the seawaters and within the sediments regulates the distribution of $CaCO_3$ across the seafloor sediments. Generally, there are mainly three types of $CaCO_3$ dissolution processes from the sea surface to the seafloor. (1) the dissolution within the seawaters. About 60–80% of $CaCO_3$ dissolved in the water depth above the chemical lysocline due to biological activities (Milliman et al. 1999); (2) the dissolution on the sediment surface. This type of dissolution occurs on the seafloors below the lysocline where carbonate is undersaturated (Peterson 1966, Archer 1996); (3) The dissolution within sediments. The combustion of organic materials produces and releases CO_2 into the pore water, which results in $CaCO_3$ dissolution within the sediments (Berger 1970).

The water depth of the transition zone in the ocean affects the $CaCO_3$ distribution in the seafloor sediments. The transition zone in the oceans is an area that below lysocline and above carbonate compensation depth (CCD), spanning several hundreds of meters in water depth. The zone above the transition zone is rich in $CaCO_3$ while the zone beneath it is almost entirely devoid of $CaCO_3$ (Archer 1996). Therefore, the regions with high $CaCO_3$ content are mostly located on the shallow ocean ridges, and the deep oceans below the CCD are always utterly devoid of $CaCO_3$.

3. Objectives and purposes of the dissertation

Ocean acidification caused by the oceanic uptake of CO_2 from atmosphere lowers the acidity of the seawaters and alters the carbonate chemistry in the oceans. The process affects the marine environments not only on the shallow but also on the deep since the ocean circulation connects these two parts.

Although most of the adsorption of atmospheric CO_2 into the oceans occurs in the relatively shallow seawaters, the influence of ocean acidification will spread to the deep counterpart (Caldeira and Wickett 2003). The deep-sea below the CCD is more susceptive due to the almost complete dissolution of carbonate, which could play the role as a natural buffer to the acidity changes of the bottom water. On the other hand, many marine organisms in the surface ocean, such as foraminifera and coccolithophorid, uptake CO_3^{2-} and secrete their shells, acting as a "biological pump" to export carbonate into the deep oceans. The lowering of carbonate ion concentration ($[CO_3^{2-}]$) in the surface seawaters caused by ocean acidification affects the biological carbonate formation and in turn the carbon cycle (Figure 1.1). This dissertation investigated the influence of ocean acidification on the deep-sea Fe–Mn nodules and planktonic foraminifera.

3.1 Ocean acidification alters the pH: Influence on the deep-sea Fe–Mn nodules

DIC can act as a natural buffer to regulate seawaters within a relatively narrow acidity range (Zeebe and Wolf-Gladrow 2001; Raven et al. 2005); however, sediments in deep oceans

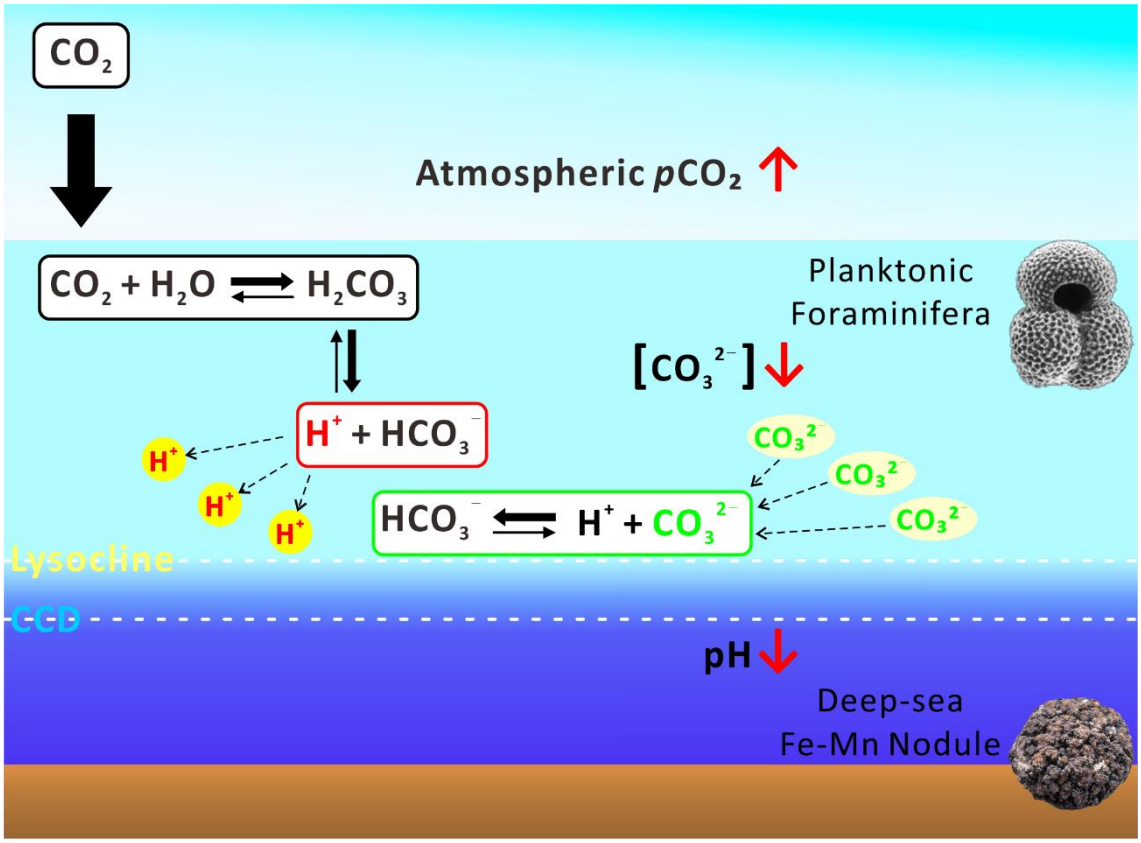

Figure 1.1 The process of ocean acidification and the influence on shallow and deep oceans.

below the CCD are often completely devoid of carbonate particles (Archer 1996; Ridgwell and Zeebe 2005). Deep-sea environments below the CCD are more vulnerable to decreasing pH. Although the impacts of ocean acidification on calcification of marine organisms and chemical speciation of the seawaters have been estimated (Millero et al. 2009; Kawahata et al. 2015), the potential influence of decreasing pH on the behavior of metals bound to deep-sea sediments such as ferromanganese (Fe–Mn) nodules is still unknown.

Deep-sea Fe–Mn nodules precipitate mainly across the deep seafloor characterized by low sedimentation rates (i.e., < 5 mm ka^{-1}) where inputs of calcareous ooze, turbidity flows, and volcanic ash is rare (Glasby 2006). The nodules with the highest grade occur on pelagic clay and siliceous ooze far from land and near or below the CCD (Glasby 1991; Verlaan et al. 2004). They occur worldwide and are found in most major oceanic basins. Their distribution is also related to the patterns of oceanic bottom water flow and, to a lesser extent, to the availability of potential nuclei on which they grow such as weathered volcanic rock, pumice, whales' ear-bones, sharks' teeth, fragments of older nodules and indurated sediment. Deep-sea Fe–Mn nodules have been intensively studied since their discovery, and a large amount of data on the geochemical composition of these marine precipitates from many locations in the world oceans is available (i.e., Koschinsky and Halbach 1995, and the references therein). Fe–Mn nodules are currently being explored and evaluated as potential targets of deep-sea mining due to their high contents of various metals such as Fe, Mn, Cu, Co, Ni, Pt, Zr, Hf, Nb, Ta, Mo, W, Te and rare earth elements (REEs) (Hein et al. 2013).

The extension of ocean acidification to deep oceans would profoundly affect the deep-sea geochemical environments, as well as the sedimentary environment of deep-sea Fe–Mn nodules. It has been reported that decreasing pH will result in changes in the behavior and fate of metals in seawater and sediments (Caldeira and Wickett 2003; Raven et al. 2005). A reduction in the pH of seawater may release previously bound metals from the deep-sea sediments into the water column and, hence, cause metal release and toxicity in the deep-sea environments (Millero et al. 2009; De Orte et al. 2014).

Chapter 2 focuses on estimating the potential influence of pH decreasing caused by ocean acidification on deep-sea Fe–Mn nodules. In this part, two types of deep-sea sediments (Fe–Mn nodule and pelagic clay) are treated in phosphate buffer solutions and artificial seawater with predicted future pH values.

3.2. Ocean acidification changes the [CO_3^{2-}]: Influence on the planktonic foraminifera

Marine organisms, such as coral reefs, coccolithophorids, and foraminiferas, build up their shells by using carbonate ion from the ambient seawaters. Foraminiferas is one of the most abundant testate protists in the world's ocean, and their shells account for a significant portion of the inorganic carbon deposit on the seafloor (Langer 2008). Planktonic foraminifera shells transfer and deposit about 32–80% of the total calcium carbonate ($CaCO_3$) preserved in deep-sea surface sediments (Schiebel 2002). A variation in the calcification rate of planktonic foraminifera shells may have a significant impact on the global carbon cycle.

The size-normalized weight of foraminiferas has been used to reflect the variation of foraminiferal calcification rate in response to the surface carbonate system (Bijma et al. 2002; Mekik and Raterink 2008; Moy et al. 2009; Naik et al. 2010; Marshall et al. 2013; Marshall et al. 2015; Osborne et al. 2016). However, some studies suggested that other environmental variables such as optimum growth conditions and carbonate saturation state of the bottom waters may also affect the observed size-normalized weight of foraminiferal shells. On the other hand, another essential but pendent issue is what the size-normalized weight accurately represents. The answer to this issue may have significant implications for paleoceanographic applications of planktonic foraminiferal shell chemistry.

Chapter 3 uses weight and size measurements and X-ray microcomputed tomography (XMCT) to investigate the influence of [CO_3^{2-}] variation caused by ocean acidification on the shells of planktonic foraminifera *Globigerinoides ruber* (white).

Chapter 2

Influence of ocean acidification on deep-sea Fe–Mn nodules: Results from leaching experiments by using phosphate buffer solutions and artificial seawater

Abstract

With the continuous rise in CO_2 emissions, the pH of seawater may decrease extensively in the coming centuries. Deep-sea environments are more vulnerable to decreasing pH since sediments in deep oceans below the carbonate compensation depth (CCD) are often completely devoid of carbonate particles. In order to assess the potential risk of metal release from deep-sea sediments in response to pH decrease in seawater, the mobility of elements from ferromanganese (Fe–Mn) nodules and pelagic clays was examined. Two geochemical reference samples (JMn-1 and JMS-2) were reacted with phosphate buffer solutions and pH-controlled artificial seawater (ASW) using a CO_2-induced pH regulation system. The experiments demonstrated that deep-sea sediments have weak buffer capacities by acid–base dissociation of surface hydroxyl groups on metal oxides/oxyhydroxides and silicate minerals. Element concentrations in the ASW were mainly controlled by elemental speciation in the solid phase and sorption–desorption reaction between the charged solid surface and ion species in the ASW. These results indicated that the release of heavy metals such as Mn, Cu, Zn and Cd should be taken into consideration when assessing the influence of ocean acidification on deep-sea environment.

1. Introduction

Since the pre-industrial era, the level of atmospheric CO_2 has increased from approximately 280 ppmv to nearly 400 ppmv (Doney et al. 2009; NOAA 2018). Driven by fossil fuel combustion, deforestation and cement manufacturing, the observed increase is at least one to three orders of magnitude faster than has occurred previously for millions of years (Sabine et al. 2004; Doney and Schimel 2007). The increasing concentration of atmospheric CO_2 is mitigated by oceanic uptake, making the surface layer of seawater more acidic. Since the Industrial Revolution, the oceans have taken up approximately 50% of the anthropogenic CO_2, lowering the average pH of the surface oceans by about 0.1 units, equivalent to a 30% increase in the concentration of hydrogen ions (Caldeira and Wickett 2003; Key et al. 2004; Raven et al. 2005; Kump et al. 2009). Absorption of anthropogenic CO_2, increased acidity, reduced pH, and lowered calcium carbonate saturation in surface seawaters, have led to the process of ocean acidification that has been well demonstrated from a series of simulations, hydrographic surveys, and time series data (Caldeira and Wickett 2003, 2005; Feely et al. 2004; Orr et al. 2005; Feely et al. 2013).

The ocean surface is in close contact and exchange with the atmosphere. Most of the anthropogenic CO_2 absorbed by the oceans still resides in relatively shallow waters; however, surface seawaters are slowly mixing with the intermediate and deep seawaters of the oceans. Over time this acidification effect will spread to the deep oceans. Caldeira and Wickett (2005) simulated ocean pH changes for the period of 2000-2100, using an ocean general circulation

model using observed atmospheric CO_2 concentration from 1975 to 2000. Their results indicated that the stabilization of atmospheric CO_2 concentration at 450 ppmv produces both calcite and aragonite undersaturation in most of the deep oceans. Ilyina and Zeebe (2012) also suggested that undersaturation will extend from the ocean floor up to 100-500 m depth over the next century. With the continuous rise in CO_2 emissions, the pH of surface seawaters will decline further, potentially from 8.1 to 7.4, while the pH reduction of the deep-sea counterpart will be about 0.4 units, declining from about 7.6 to 7.2 (Caldeira and Wickett 2003). Dissolved inorganic carbon (DIC) can act as a natural buffer to regulate seawaters within a relatively narrow acidity range (Zeebe and Wolf-Gladrow 2001; Raven et al. 2005); however, sediments in deep oceans below the CCD are often completely devoid of carbonate particles (Archer 1996; Ridgwell and Zeebe 2005). Therefore, deep-sea environments are more vulnerable to decreasing pH. Although the impacts of ocean acidification on calcification of marine organisms and chemical speciation of the seawaters has been estimated (Millero et al. 2009), the potential influence of decreasing pH on the behavior of metals bound to deep-sea sediments such as Fe–Mn nodules is still unknown.

Deep-sea metallic sediments, such as Fe–Mn nodules and crusts, are currently being explored and evaluated as potential targets of deep-sea mining due to their high contents of various metals such as Fe, Mn, Cu, Co, Ni, Pt, Zr, Hf, Nb, Ta, Mo, W, Te and rare earth elements (REEs) (Hein et al. 2013). Fe–Mn nodules lie on the abyssal plains at any water depth, but the highest-grade nodules form near or below the CCD (Verlaan et al. 2004; Glasby

2006). Fe–Mn crusts precipitate on the surface and flanks of seamounts, ridges, and plateaus as pavements and coatings on rock outcrops, where near-bottom currents have swept the seafloor clear of sediment for millions of years. The extension of ocean acidification to deep oceans would profoundly affect the deep-sea geochemical environments, as well as the sedimentary environment of deep-sea Fe–Mn deposits. It has been reported that decreasing pH will result in changes in the behavior and fate of metals in seawater and sediments (Caldeira and Wickett 2003; Raven et al. 2005). A reduction in the pH of seawater may release previously bound metals from the deep-sea sediments into the water column and, hence, cause metal release and toxicity in the deep-sea environments (Millero et al. 2009; De Orte et al. 2014).

2. Leaching experiments by using phosphate buffer solutions

2.1. Materials

Geochemical reference materials JMn-1and JMS-2 were used for leaching experiments. JMn-1 is a sample of Fe–Mn nodules collected from the ocean floor of the southern Central Pacific Basin in 1982 (Terashima et al. 1995). It mainly consists of buserite (an unstable manganese oxide that dehydrates to birnessite), with a minor amount of vernadite (low-crystalline Fe–Mn oxide) and silicate minerals. JMS-2 is a sample of deep-sea sediments collected from the Penrhyn Basin, South Pacific in 1983. The sediment is composed of pelagic clay, with minor amounts of calcareous and siliceous components (Terashima et al.

2002). The most dominant clay mineral is montmorillonite. Philipsite, plagioclase and quartz were also identified as crystalline phases. Detailed sample processing has been described in elsewhere (Terashima et al. 1995, Terashima et al. 2002).

2.2. Leaching experiments

Solutions of 0.2 M sodium dihydrogen phosphate (NaH_2PO_4) and 0.2 M sodium hydrogen phosphate (Na_2HPO_4) were prepared and used to produce buffer solutions with different pH values. 47.35ml, 43.50ml, and 30.50ml of 0.2 M NaH_2PO_4 were respectively mixed with 2.65ml, 6.50ml, and 19.50ml of 0.2 M Na_2HPO_4. These solutions were then diluted to 100ml using distilled water. The initial pH values were 8.1/8.2, 7.7/7.8 and 7.1 (NBS scale), respectively (Table 2.1).

One gram each of JMn-1 and JMS-2 was placed into separate 100 ml screw cap polypropylene bottles, and then mixed with 100 g of phosphate buffer solution. Samples were kept in a thermostatic bath (25°C) for 24 hours and/or 120 hours and stirred with a magnetic stirrer (Figure 2.1). Residues and leachates were then separated using surfactant-free cellulose acetate (SFCA) filters (Sartorius, 0.2 μm pore size). The first 30 ml of leachate were not collected, but rather used to wash the filters. Phosphate buffer solutions were filtered in the same way for preparing the buffer blanks. Filtered leachates and buffer blanks were acidified with ultrapure HNO_3 (Kanto Chemical Co. Inc.) and stored in acid-clean polypropylene bottles at 4°C. The procedures follow the method by Gupta et al. (2005).

	Sample	JMn-1							JMS-2				Filtered buffer blanks (n=9)	Bulk of JMn-1*	Bulk of JMS-2*
	Time	24 hours			120 hours				24 hours						
	T(°C)	25			25				25						
	Initial pH	7.1	7.7	8.1	7.1	7.8	8.2		7.1	7.7	8.1				
	Final pH	7.5	8.2	8.6	7.5	8.3	8.6		7.1	7.8	8.2		average	(μg/g)	(μg/g)
Group 1	Li	103	55.5	39.3	102	55.2	38.5		9.72	7.92	7.02		0.06	71.7	43
	B	675	596	576	685	623	604		210	196	185		2.41	138	106
	Mg	2970	1580	1040	2930	1560	1080		19400	15500	12500		0.77	18800	19500
	Si	14000	10500	9230	16200	12100	10600		16200	11400	8870		37.4	65900	195000
	Sc	2.1	1.58	1.41	2.41	1.81	1.6		2.69	1.88	1.5		0.04	13	27.1
	Sr	15	7.26	4.68	14.4	7.04	5.01		57.3	40.5	29.4		0.01	792	454
	Ba	0.05	0.03	0.02	0.06	0.03	0.02		0.17	0.15	0.11		0.03	1710	1860
	Tl	0.16	0.15	0.13	0.18	0.15	0.13		0.09	0.1	0.09		b. d.	161	2.82
	U	0.01	b. d.	b. d.	0.01	b. d.	b. d.		0.05	0.04	0.04		b. d.	5	2.8
Group 2	Al	2.25	3.43	5.58	2.35	3.74	5.7		27.5	20.8	19.3		1.44	22800	75000
	Cr	1.02	0.98	1	1.03	1.01	1.01		7.38	7.12	6.84		0.07	26.6	78
	Mn	0.45	0.42	0.44	0.33	0.31	0.3		3.38	1.34	0.91		0.81	256000	17500
	Fe	5.26	1.73	2.05	3.5	b. d.	b. d.		34.1	21.9	14.4		b. d.	101000	76700
	Ni	0.03	b. d.	b. d.	0.03	b. d.	b. d.		5.04	2.07	1.2		0.1	12600	311
	Zn	0.2	0.12	0.42	0.15	0.11	0.1		0.57	0.61	1.18		0.17	1070	166
	Pb	0.02	0.02	0.02	0.02	0.02	0.02		0.06	0.07	0.14		0.02	430	88
Group 3	V	84.9	123	161	93.2	144	192		64.4	66.2	69.6		0.02	424	183
	Cu	4.03	4.13	4.88	4.27	5.1	6.49		7.35	7.25	6.78		2.06	11100	447
	Mo	232	274	280	328	474	505		84.2	81.7	76.5		0.01	318	25.4
	Cd	0.23	0.28	0.28	0.31	0.49	0.51		0.09	0.08	0.07		b. d.	15.5	0.48
	W	1.32	2.27	2.72	1.58	3.14	4.27		6.03	6.33	5.86		0.01	45.3	6.34

units are in ng/g except where indicated otherwise

b. d. below detection limit

*Terashima, 1995, 2002; Awaji, 2009

Table 2.1 Experiment conditions, element concentrations of leachates (before filtered buffer blank subtraction), average element concentrations of filtered buffer blanks and element abundance in bulk of JMn-1 and JMS-2. (chemical compositions of JMn-1 and JMS-2 are from Terashima et al. 1995, 2002 and Awaji 2009)

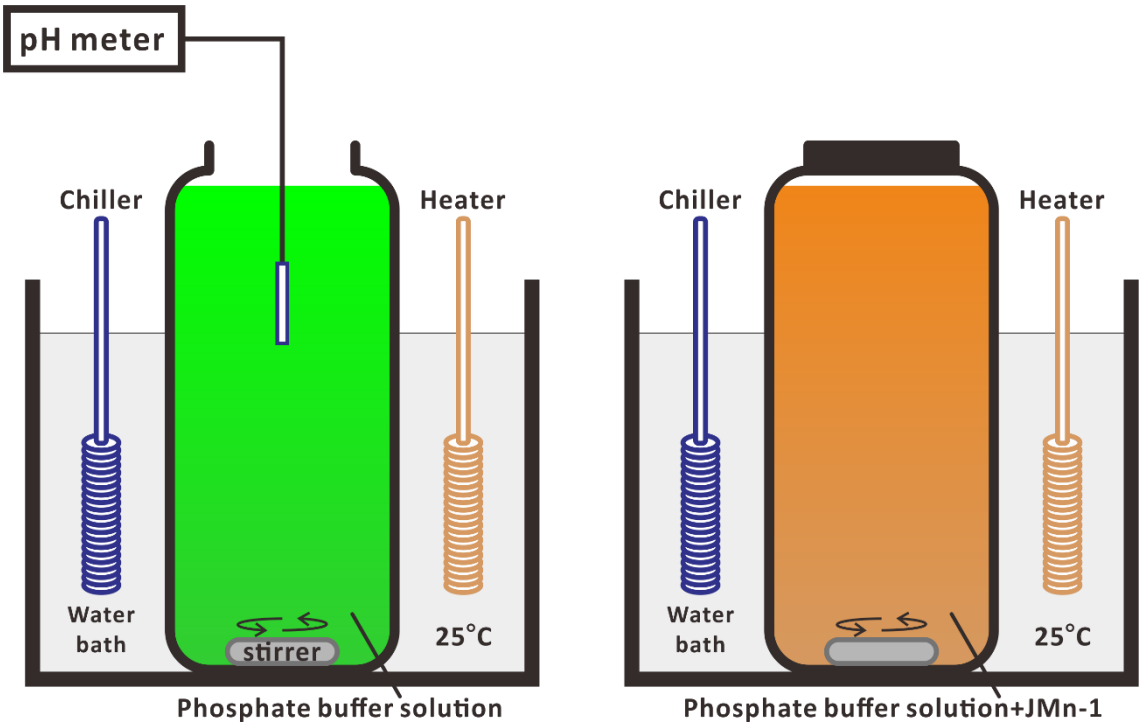

Figure 2.1 Leaching experiment settings by using phosphate buffer solutions to regulate the acidity of the solutions.

Element concentrations of leachates were then analyzed by ICP-MS (7700x, Agilent Technologies, USA) at the Geological Survey of Japan, National Institute of Advanced Industrial Science and Technology, Japan. In order to subtract the background and to calculate the net concentrations of leachates, element concentrations of filtered buffer blanks were analyzed as well. Analytical error during the ICP-MS measurement was typically <±3% RSD (error was <±5% RSD for Cu, Zn, Pb and <±10% RSD for Fe) at element concentrations of 10 ng/g.

Although buffer solutions were used as solvents in this study, final pH values (pH of leachates) were slightly different from the initial values (pH of phosphate buffer solutions). Prior to this experiment, pH values of mixtures measured 10 minutes after mixing were the same as those after 24 and/or 120 hours. Therefore, we used final pH values.

2.3. Metal precipitation examine

In the leaching experiments by using phosphate buffer solutions, chemical co-precipitation reactions between phosphate anions and elements dissolved in solution may affect sorption-desorption processes. Some metals may react with phosphate ion (PO_4^{3-}) and probably result in co-precipitation. Visual Minteq software was used to estimate the ion activation product and saturation index and examine the possible metal precipitations in the phosphate solutions.

2.4. Result of phosphate buffer solution experiment

Element concentrations of leachates and average element concentrations of filtered buffer blanks are shown in Table 2.1. Net element concentrations of leachates were obtained by subtracting the average element concentrations of filtered buffer blanks (n=9) from the analyzed element concentrations of leachates. Most of the elements showed clear variation as the pH of the mixtures decreased from weakly alkaline to near neutral value. Specifically, element concentrations of Li, B, Mg, Si, Sc, Sr, Ba, Tl, and U increase with a decreasing pH from weakly alkaline to near neutral value. Concentrations of Al, Cr, Mn, Fe, Ni, Zn, and Pb in JMn-1 showed no observable increase or decrease, while concentrations of leachates from JMS-2 showed distinct increases except for a slight decrease of Zn and Pb. Concentrations of V, Cu, Mo, Cd, and W in JMn-1 showed an obvious reduction as pH decreases, but elements in leachates of JMS-2 showed no significant variation in element concentrations under different acidity conditions.

3. Leaching experiments by using artificial seawater

3.1. Artificial seawater

In seawater carbonate chemistry research, seawater is treated as a constant ionic medium in which the thermodynamics of various chemical processes involving minor constituents can be studied. Artificial seawater (ASW) is often used rather than natural seawater to minimise biological effects and to provide reproducible solutions of known composition.

Kester et al. (1967) developed a method for reproducible and satisfactory ASW that agrees well with the composition of natural seawater. To simplify the recipe, Dickson (1990) replaced HCO_3^-, Br^-, BO_3^{3-} and F^- with Cl^- and Sr^{2+} with Ca^{2+}. This modified recipe is the basis of the ASW that has been used to determine a variety of equilibrium constants for use in seawater research (Roy, et al. 1993).

In this study, ASW was produced according to Dickson's simplified recipe using 24.9372 g kg-H_2O^{-1} NaCl, 11.1042 g kg-H_2O^{-1} $MgCl_2 \cdot 6H_2O$, 4.1484 g kg-H_2O^{-1} Na_2SO_4, 1.1904 g kg-H_2O^{-1} $CaCl_2$ (anhydrous), 0.7870 g kg-H_2O^{-1} KCl (Wako Chemical, Osaka, Japan). In addition, 0.2029 g kg-H_2O^{-1} $NaHCO_3$ (Kanto Chemical. Tokyo, Japan) was added to keep the pH buffer capacity at the level of natural seawater, as specified by Kester et al. (1967).

Before adding Fe–Mn nodule or pelagic clay samples, the pH values of ASW samples were adjusted to cover the predicted pH range of natural seawater caused by ocean acidification (8.1 to 7.2) by altering the partial pressure of CO_2 of ASW via CO_2 or CO_2-free-air aeration. The CO_2-free-air was produced by removing CO_2 from the air stream by soda lime. The pH of each ASW sample was adjusted to a specific value (for example, the initial pH of ASW samples were adjusted to 8.41, 8.08, 7.69, 7.38, 7.05, 6.92 when solid-to-liquid (S/L) ratio was set to 1/1000). When the pH was higher than the specific value, CO_2 aeration was performed, and when the pH dipped lower than the specific value, CO_2-free-air aeration was executed (Figure 2.2).

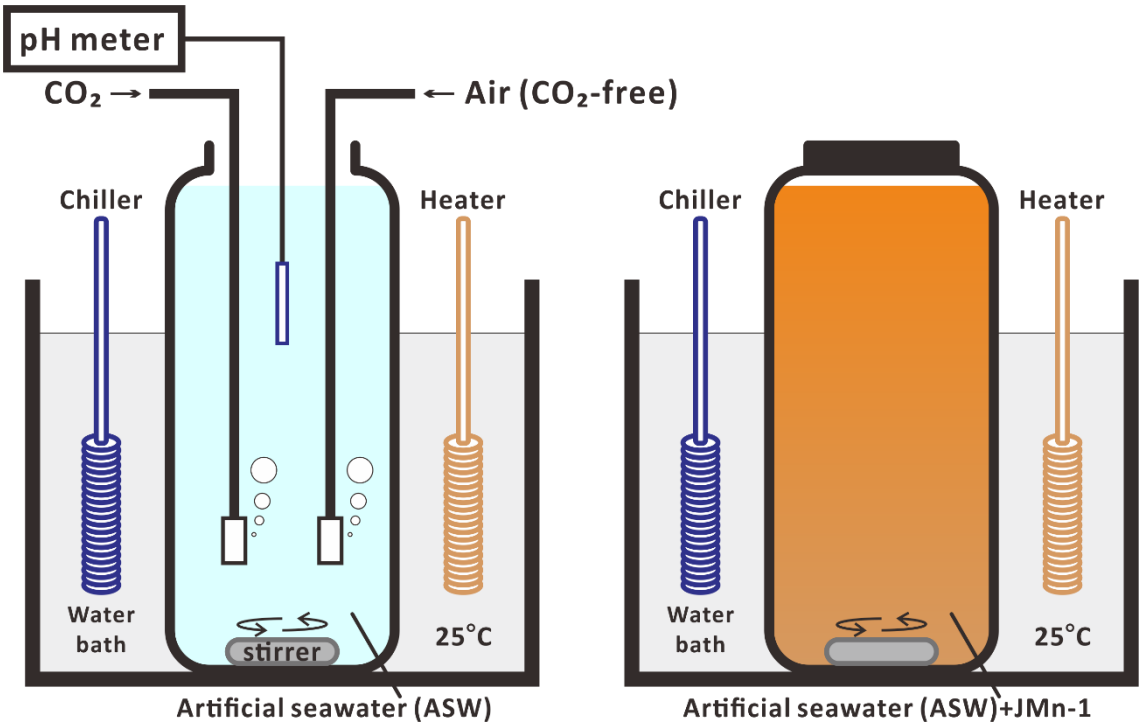

Figure 2.2 Leaching experiment settings by using artificial seawater. The CO_2 or CO_2-free-air aeration is used to adjust the acidity of the solutions

3.2. Experiments

All glassware and Teflon vials used for sample treatment were leached in 10% HNO_3 (Tamapure, Tama Chemicals, Tokyo, Japan) at room temperature for 12 hours and then rinsed three times with ultra-pure water of 18.2 MΩ cm^{-1} quality (system: Elix 3, Milli-Q plus, Millipore). The JMn-1 and JMS-2 samples were carefully weighed and placed into separate screw-cap glass bottles (borosilicate glass bottles and polypropylene caps, AS ONE), and then mixed with ASW in a S/L ratio of 1/100, 1/1000, and 1/10,000. The bottles were kept in a thermostatic bath (25°C) and stirred with a magnetic stirrer (Gupta, et al. 2005; Wang, et al. 2017). The experiments were carried out under in-door condition without daylight or artificial illumination (Figure 2.2). After 24 hours, the ASW samples were separated using surfactant-free cellulose acetate (SFCA) filters (Sartorius, 0.45 μm pore size). The first 20 ml of filtered ASW were not collected, but were used to wash the filters and for pH measurements. Filtered ASW samples were acidified with ultra-pure HNO_3 (Tamapure, Tama Chemicals, Tokyo, Japan) and stored in Teflon bottles at 4°C.

3.3. pH measurements

The pH measurements followed the procedures described by Dickson et al. (2007). The pH values of the ASW were determined by measurements of a glass/reference electrode cell (Metrohm, Swiss). Standard pH buffer solution values (2-amino-2-hydroxymethyl-1,3-propanediol "TRIS," and 2-aminopyridine "AMP") were then assigned. All sample

containers were tightly closed during pH measurements to avoid air exchange with the atmosphere, and the temperature was maintained at 25°C (±0.1 °C). After adjusting the acidity of ASW via the CO_2-induced pH regulation system and before adding Fe–Mn nodule or pelagic clay samples, pH values of ASW were measured. These pH values are called "initial pH". At the end of the experiments, pH values were measured immediately after filtration of the ASW samples. These pH values are called "final pH". Before the experiment we conducted a series of testing experiments to observe the pH drifting. pH of ASW samples drifts within 30 minutes after adding Fe–Mn nodule or pelagic clay samples, but thereafter it almost keeps stable. The pH values measured 30 minutes after adding Fe–Mn nodule or pelagic clay samples are the same as the "final pH" (pH measured 24 hours later). Therefore, we used final pH values in discussions.

3.4. ICP-MS measurements on artificial seawater samples

To reduce spectral interferences and to avoid interface cone clogging, sample pre-dilution and reaction/collision cell are introduced to improve the performance of ICP-MS measurements on seawater samples (Leonhard et al. 2002; McCurdy and Woods 2004; Grotti and Frachea 2007). In this study, the multi-elements concentrations were analysed in the filtered ASW samples by ICP-MS (7700x, Agilent Technologies, USA) at the Geological Survey of Japan, National Institute of Advanced Industrial Science and Technology, Japan. All samples were diluted 20 times by adding 2% HNO3 (Tamapure, Tama Chemicals, Tokyo,

Japan), in which 10 ng/g each of Be, Sc, Y, and Tl were added as internal standards to control matrix effects and correct for instrumental drift. To approximate the matrix of these 20-times-diluted samples, the calibration standards were prepared by adding multi-element standard solutions XSTC-622 (SPEX Certi-Prep, USA) into 20-times-diluted ASW blanks. All the measurements were corrected using internal standards as follows: Be was used to correct Li and B, Sc to correct Al through As, Y to correct Rb through Ba, and Tl to correct W and U. Li, B and Al were measured on standard mode (No Gas mode); V, Cr, Mn, Cu, Zn, Ga, As, Rb, Mo, Ag, Cd, Sb, Cs, Ba, W and U were measured on Helium gas mode. Detection limit of all elements is below 0.01ng/g except for B (0.02 ng/g). Analytical error during the ICP-MS measurement was typically <±2.5% RSD (error was <±5% RSD for Al and Zn) at element concentrations of 10 ng/g.

3.5 Result of artificial seawater experiment

The pH measurements are presented in Table 2.2. Final pH values drifted from the initial pH values that were taken before the addition of JMn-1 or JMS-2. At a S/L ratio of 1/10,000, the final pH values only drifted within 0.05 of their initial values. When the S/L ratio was 1/1000, the pH drifted further from the initial values. The pH drift was negligible (within 0.01) for the JMn-1 trials when the initial pH was set to 7.38. ASW samples in the JMn-1 trials with a lower initial pH experienced a pH increase, whereas ASW samples with a higher initial pH experienced a pH decrease. Negligible pH drifting occurred in the JMS-2 trials

S/L ratio	Sample	Initial pH	Final pH
1/10000	JMn-1	7.14	7.17
		7.71	7.67
		8.21	8.17
	JMS-2	7.14	7.21
		7.71	7.69
		8.21	8.20
1/1000	JMn-1	6.92	7.09
		7.05	7.23
		7.38	7.37
		7.69	7.60
		8.08	7.87
		8.41	8.11
	JMS-2	6.92	7.21
		7.05	7.29
		7.38	7.46
		7.69	7.70
		8.08	8.02
		8.41	8.33
1/100	JMn-1	8.57	7.47
	JMS-2	8.57	7.92

Table 2.2 pH values before and after the addition of the JMn-1/JMS-2 samples to the ASW. Initial pH refers to the pH value of the ASW immediately following CO_2 or CO_2-free-air aeration. Final pH refers to the pH value of the ASW measured immediately after filtration of the ASW samples at the end of the experiments.

with an initial pH of 7.69. However, similar to the JMn-1 trials, trials with higher initial pH values saw a pH increase and trials with lower initial pH values saw a pH decrease. At the highest S/L ratio, 1/100, the drift from initial pH values was pronounced. JMn-1 samples saw a pH decrease of 1.1 (from 8.57 to 7.47) and JMS-2 samples saw a pH decrease of 0.65 (from 8.57 to 7.92). pH values of the ASWs varied according to the S/L ratio and initial pH values, and these changes reached equilibrium within 30 minutes. Therefore, final pH values obtained at the equilibrium were used (Wang, et al. 2017). Due to the substantial pH change during the trials with a S/L ratio of 1/100 and the high dilution factor during the trials with a S/L ratio of 1/10,000, the discussions presented in the next section focus mainly on the trials with a S/L ratio of 1/1000.

As the ASW samples were diluted 20 times before ICP-MS measurement, Table 2.3 presents the adjusted ICP-MS data after multiplication by a factor of 20. The concentrations of Li, Mn, Cu, Zn, Ga, Cd and Ba increased as the ASW acidified from weak alkaline to near neutral. On the contrary, the concentrations of Al, V, Cr, As, Rb, Mo, Ag, Sb and W decreased as the pH declined. The concentrations of B, Cs and U did not present any clear trends with the pH decreases.

S/L ratio	1/1000									1/10000								1/100			Bulk of	Bulk of
Sample	JMn-1					JMS-2				JMn-1				JMS-2				JMn-1	JMS-2		JMn-1	JMS-2
Final pH	8.11	7.87	7.6	7.37	7.23	7.09	8.33	8.02	7.7	7.46	7.29	7.21	8.17	7.67	7.17	8.2	7.69	7.21	7.47	7.92	* (μg/g)	* (μg/g)
Li	14.8	15.9	18.2	20.7	23	23	2.13	2.11	2.14	2.12	2.21	2.28	1.93	2.17	2.58	0.16	0.15	0.13	134	19.1	71.7	43
B	87.5	120	122	110	89.1	142	54	59.3	44	44.7	48.3	47.7	23.2	12	21	15.4	8.5	10.1	972	635	138	106
Al	33.5	0.91	3.06	2.07	1.85	1.35	12.7	11.5	9.45	7.07	3.69	3.25	2.28	1.66	2.06	22.9	10.2	2.84	1.42	5.02	22800	75000
V	2.88	3.17	1.84	1.47	0.9	1.02	3.3	2.21	1.63	1.55	1.3	1.16	2.11	1.03	0.87	1.03	0.65	0.59	2.04	2.95	424	183
Cr	0.56	b.d.	0.11	0.18	b.d.	b.d.	0.97	0.75	0.45	0.77	1.1	0.54	0.03	b.d.	b.d.	b.d.	b.d.	0.17	1.09	7.31	26.6	78
Mn	0.25	b.d.	0.14	b.d.	0.64	0.07	b.d.	b.d.	0.9	2.3	5.58	5.33	b.d.	b.d.	0.16	0.46	1.99	5.41	b.d.	b.d.	256000	17500
Cu	0.33	0.34	0.54	0.42	0.7	0.72	0.24	0.21	0.21	0.45	0.32	0.29	0.07	0.2	0.44	b.d.	0.01	0.14	0.27	0.43	11100	447
Zn	4.27	2.12	4.92	3.28	11	5.03	8.64	8.63	8.36	9.26	12.1	10.3	b.d.	0.53	1.59	2.7	1.48	2.18	0.79	3.62	1070	166
Ga	3.02	3.69	7.36	4.07	4.95	5.43	14.8	15.7	17	15	16.4	17.6	0.37	0.28	1.19	2.61	2.38	2.48	1.11	5.79	37.1	17.8
As	1.03	1.26	0.52	0.23	0.11	0.11	1.29	1.41	0.91	0.91	0.61	1.02	0.37	0.16	b.d.	0.14	b.d.	0.04	0.74	1.39	75.4	35
Rb	2.84	2.59	2.85	2.88	2.4	2.15	8.93	8.44	8.7	7.88	8.53	8.62	b.d.	b.d.	b.d.	0.64	0.92	0.8	17	42.4	10.9	65
Mo	30.6	22.2	16.2	11.3	6.53	5.28	6.9	6.91	6.42	5.96	4.95	4.74	3.75	2.99	2.68	1.02	0.94	0.74	28.9	53.4	318	25
Ag	5.37	2.26	2.63	1.43	1.75	b.d.	6.83	2.27	7.75	b.d.	b.d.	b.d.	b.d.	b.d.	b.d.	b.d.	b.d.	b.d.	1.29	7.71	—	—
Cd	0.3	0.17	0.37	0.4	0.4	0.42	0.03	0.04	0.07	0.11	0.09	0.13	0.11	0.19	0.17	0.02	0.05	0.04	0.49	0.29	15.5	0.48
Sb	0.86	0.68	0.52	0.55	0.48	0.51	0.51	0.65	0.44	0.37	0.12	0.08	0.55	0.1	0.39	0.36	0.04	0.35	0.64	0.81	37.5	5
Cs	0.06	0.04	0.04	0.04	0.04	0.05	0.13	0.15	0.15	0.12	0.14	0.14	0.01	0.02	0.01	0.04	0.03	0.04	0.09	0.19	0.6	3
Ba	17.2	26	49.1	25.3	30.8	36.6	96.9	99.3	116	103	109	116	2.5	2.38	7.25	17.8	16.1	16.9	7.06	37.5	1710	1860
W	0.41	0.21	0.17	0.11	0.02	0.04	0.44	0.24	0.15	0.04	0.07	0.02	b.d.	b.d.	b.d.	b.d.	b.d.	b.d.	0.06	0.46	45.3	6.34
U	0.28	0.23	0.2	0.23	0.26	0.23	0.16	0.14	0.18	0.13	0.15	0.16	0.03	0.04	0.05	0.02	0.03	0.03	0.18	0.38	5	2.8

Units are in ng/g except where indicated otherwise

S/L ratio: solid-to-liquid ratio

b.d.: below detection limit

* Terashima et al. (1995, 2002) and Awaji (2009)

Table 2.3 Elemente concentrations in the filtrate ASW sample after 24 hours of exposure of JMn-1/JMS-2 to different pH conditions. The concentrations are presented after adjusting for sample dilution in nitric acid by multiplying by a factor of 20. (chemical compositions of JMn-1 and JMS-2 are from Terashima et al. 1995, 2002 and Awaji 2009)

4. Discussion

4.1. Chemical co-precipitation in the phosphate buffer solution experiments

The ion activation product and saturation index of metals in the leachates of phosphate buffer solution experiment were calculated according to the metal concentration obtained by the ICP-MS measurements. The saturation of metals is shown in Table 2.4. In 0.1 M of phosphate buffer solutions, Al, Cu, Fe, Mg, Mn, Pb, and V tend to co-precipitate with PO_4^{3-} at all pH values in our experiment, while other elements seem to be not affected by the co-precipitation reactions with PO_4^{3-}. It infers that the element behavior of Al, Cu, Fe, Mg, Mn, Pb, and V should be different from that in the real marine environment. Therefore, we do not use the concentration of these elements for discussion the influence of pH changes on the metal release from deep-sea sediments. The trend of other elements agrees with the result of artificial seawater experiments.

4.2. pH drifting in the artificial seawater experiments

The pH of ASW fluctuated for 30 minutes after the addition of deep-sea sediments; this has rarely been documented in previous studies. The influence of deep-sea pelagic clays on the vertical pH profile in the Pacific Ocean was noted by Park (1966), but this work ascertained neither how the deep-sea sediments influenced the pH of seawater nor how far above the sea floor this influence altered the pH profile. Stumm et al. (1970) and Schindler (1975) has proposed “Surface Complex Formation Model” to describe the reactions between

Sample	JMn-1			JMS-2		
pH	7.5	8.2	8.6	7.1	7.8	8.2
Al	X	X	X	X	X	X
Ba	O	O	O	O	O	O
Cd	O	O	O	O	O	O
Cr	O	O	O	X	X	X
Cu	X	X	X	X	X	X
Fe	X	X	X	X	X	X
Li	O	O	O	O	O	O
Mg	X	X	X	X	X	X
Mn	X	X	X	X	X	X
Mo	O	O	O	O	O	O
Ni	O	O	O	O	O	O
Pb	X	X	X	X	X	X
Sc	O	O	O	O	O	O
Sr	O	O	O	O	O	O
Tl	O	O	O	O	O	O
U	O	O	O	O	O	O
V	X	X	X	X	X	X
W	O	O	O	O	O	O
Zn	O	O	O	O	O	O

X: oversaturation in 0.1M of phosphate solution

O: undersaturation in 0.1M of phosphate solution

Table 2.4 Oversaturation/undersaturation of metals in 0.1 M of phosphate solutions.

solid phases and solutions. In this model, hydroxyl groups on the surface of solid phases such as Si-OH, Mn-OH and Fe-OH are generated due to the hydrolysis of oxide surfaces once the solid phase is exposed to solutions. Boehm (1971) found that hydroxyl groups on the surface of solid phases are either acidic or basic in character, due to their structure, and the acidic and basic properties depend on the nature of the oxide in the solid phase. Surface hydroxyl groups can react with water molecules and charged ions/complexes in the solutions and release or fix H^+ or OH^- and thus influence the solution's acidity. The pH of point of zero charge (pH_{PZC}) of the solid phase determines the surface charge of the hydroxyl groups at a given pH value (Stumm and Morgan 1996). Protonation occurs when the pH of a solution is lower than the pH_{PZC} of the solid phase; consequently, H^+ ions fix to the surface hydroxyl groups, and the pH of the solution increases. Contrarily, deprotonation results in the releasing of H^+ ions from surface hydroxyl groups when the pH of the solution is higher than the pH_{PZC} of the solid phase, and consequently in the decrease of the pH of the solution.

The pH_{PZC} values of Fe–Mn nodules and pelagic clays in seawater are still unknown. Parida et al. (1996) conducted acid-base titration using a Fe–Mn nodule sample in KNO_3 supporting electrolyte and found pH_{PZC} to be ~4.5. They expected that the pH_{PZC} of Fe–Mn nodules is the average of the pH_{PZC} values of MnO_2, FeOOH, Al_2O_3 and SiO_2. In this study, the pH measurements shown that the addition of JMn-1 or JMS-2 lowered the pH of ASW samples with high initial pH values but raised the pH of samples with low initial pH values (Figure 2.3). These pH drifts are consistent with the pH regulating processes caused by pH_{PZC}

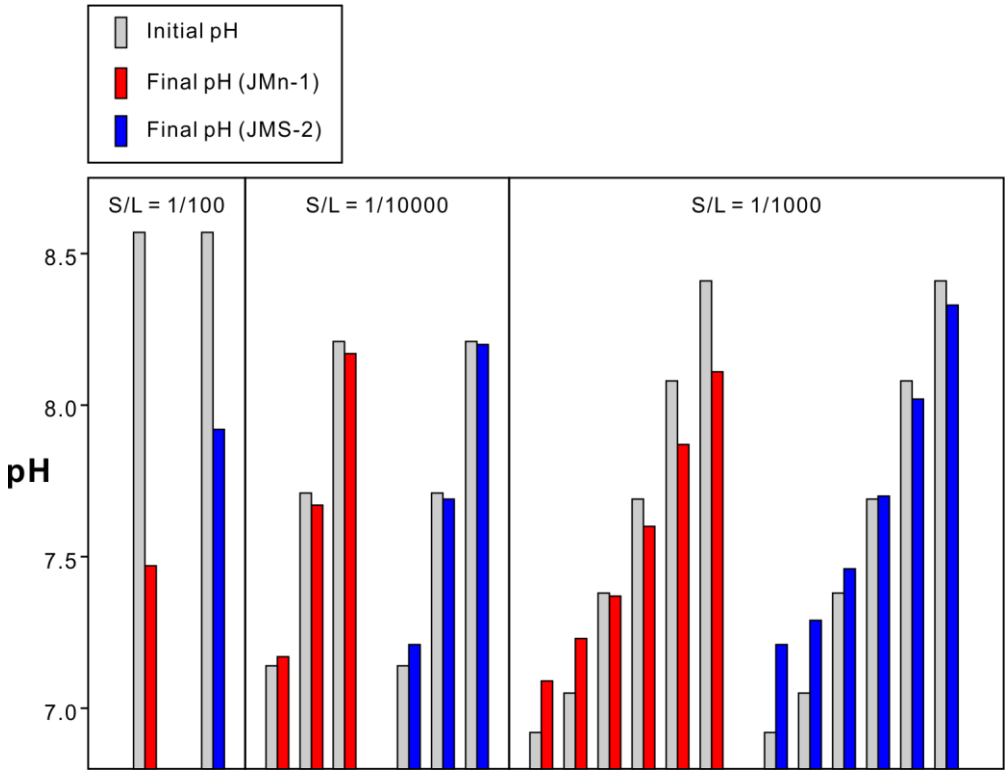

Figure 2.3 pH drifting after the addition of JMn-1 or JMS-2. The addition of JMn-1 or JMS-2 lowered the pH of ASW samples with elevated initial pH values but raised the pH values of ASW samples with lowered initial pH values.

of solid phases. Furthermore, in the experiments at a S/L ratio of 1/1000, we found the least pH drifts (0.01) when initial pH values are 7.38 for JMn-1 and 7.69 for JMS-2. Therefore, we infer that the pH_{PZC} of JMn-1 and JMS-2 in the ASW is ~7.4 and ~7.7, respectively. The pH_{PZC} value of JMn-1 in ASW is different from the observed pH_{PZC} value reported by Parida et al. (1996), this is because the observed pH_{PZC} are always influenced by the composition of the solutions. Zaman et al. (2009) also reported that the composition of solutions causes obvious pH_{PZC} shifting.

The observed buffer capacities of JMn-1 and JMS-2 may invoke the idea that deep-sea sediments are able to mitigate ocean acidification to some extent. However, considering that the ratio of total seawater mass to exposed deep-sea sediment surface is quite big, this pH buffer effect might be very limited. In addition, the observed pH drifting reached equilibrium within 30 minutes in the experiments, which indicates that surface hydroxyl groups react with seawater very rapidly. Therefore, it is suggested that the buffer process of deep-sea sediments would not influence the element mobility at long time-scale.

4.3. Elements released into the artificial seawater mainly originated from exchangeable fractions

It is untenable to evaluate the element compositions of solutions based on the total abundance of the bulk sediments, since sediments can be partitioned into five specific fractions: *Exchangeable fraction*, *Carbonate-bounded fraction*, *Fe–Mn oxide-bounded*

fraction, *Organic matter-bounded fraction* and *Residual fraction* (Tessier et al. 1979; Bayon et al. 2002), and elements in different fractions have differentiated behavior. Elements in *Exchangeable Fraction* are adsorbed onto mineral surfaces and controlled by sorption-desorption processes; *Carbonate-Bounded Fraction* are susceptible to pH changes; *Fe–Mn Oxide-Bounded Fraction* are unstable under anoxic conditions; Metals in marine environments can be bound to *Organic Matter-Bounded Fraction* through bioaccumulation processes in certain living organisms; *Residual Fraction* mainly contains primary and secondary minerals which hold trace metals within their crystal structure. Elements in this fraction are not expected to release into seawaters over a reasonable time span under normal conditions in the marine environment. Metal extraction experiments in Fe–Mn mining industries have demonstrated that strongly acidic or alkaline reagents can extract valuable metals from deep-sea Fe–Mn nodules or crusts (Kanungo and Das 1988; Charewicz et al. 2001). Compared to the pH conditions in industrial metal extraction procedures, the pH range of natural seawater is quite mild. Therefore, we infer that the elements released into the ASW should be mainly derived from the exchangeable fractions of JMn-1 and JMS-2 with concentrations mostly controlled by sorption-desorption processes. Previous studies have also reported that the process of metal enrichment in Fe–Mn nodules in marine environments is controlled by sorption-desorption mechanisms due to the high porosity and specific surface area of Fe–Mn nodules (Koschinsky and Hein 2003; Glasby 2006; Wang, et al. 2017).

4.4. pH-regulated element concentrations in artificial seawater

The sorption-desorption processes occurring between solutions and solid phases are closely related to the physical-chemical properties of the host phases and ion species in the solutions (Koschinsky and Halbach 1995; Koschinsky and Hein 2003). In the Surface Complex Formation Model, hydrolysis of the solid phase surface results in different surface charge. When pH of the solutions is below pH_{PZC} of the solid phase, protonation occurs on the solid phase surface and the surface is positively charged. Deprotonation occurs when pH of the solutions exceeds the pH_{PZC} of the solid phase and the surface becomes negatively charged. Plotting of surface charge versus pH shows a monotonically increasing trend in surface charge as pH decreases. The pH measurements shown that the pH_{PZC} of JMn-1 and JMS-2 in ASW is about 7.38 and 7.69, respectively. Therefore, the surface charge of JMn-1 and JMS-2 increase monotonically as the pH of ASW samples decreases from 8.1 to 7.2.

Coulombic electrostatic interaction has been used to explain the sorption-desorption processes between charged species in solution and host phases. Cations such as alkali and alkaline earth metals are preferentially adsorbed on the negatively charged surface, while neutral or negatively charged complexes and anions bind to the slightly positively charged surfaces (Koschinsky and Halbach, 1995; Koschinsky and Hein, 2003). As discussed above, the surface charge of JMn-1 and JMS-2 increase monotonically as the pH of ASW samples decreases from 8.1 to 7.2, therefore, according to Coulomb's law, the attractive force on positively charged ions and the repulsive force on negatively charged ions decreases

(Koschinsky and Halbach 1995; Koschinsky and Hein 2003). In other words, as the pH of the ASW changes from 8.1 to 7.2, positively charged ions in the ASW are more likely to be desorbed from the solid phases, while negatively charged ions are more easily adsorbed by the solid phases. Consequently, variations in element concentrations in the ASW are primarily determined by the ion species present in the solutions.

A compilation of dissolved inorganic elements found in seawater is shown in Table 2.5. Li, Mn, Cu, Zn, Rb, Cd, Cs and Ba exist mainly as free cations or positively charged complexes in seawater (Byrne 2002). As the pH of the seawater decreases, these elements are more likely to release from sediments; thus, their concentrations will increase, as was shown in Figure 2.4. The principal species with negatively charged ions in seawater are V, As, Mo, Ag, Sb, W and U (Byrne 2002; Endrizzi and Rao 2014). Although V and As exist in seawater in various forms, all are negatively charged. Thus, their concentration in the ASW decreased as the pH decreased. Mo and W normally take the forms of MoO_4^{2-} and WO_4^{2-}, in seawater, respectively (Byrne 2002; Millero 2013). Therefore, as solution pH decreases, they tend to be absorbed by the sediments, resulting in a decrease of their concentrations in seawater.

As the pH of ASW samples decreased, no obvious increase or decrease in concentration of Mn in ASW (JMn-1) was observed (Figure 2.4), although Mn is one of the most abundant elements in Fe–Mn nodules. This may be attributed to that Mn rarely being associated in the exchangeable fraction of Fe–Mn nodules (Koschinsky and Hein 2003). As the acidity of the

Element	Principal species	Dominant charge	Reference
Li	Li^+(98%), $LiSO_4^-$(2%)	+	Byrne 2002
B	$B(OH)_3^0$/$B(OH)_4^-$	0	Byrne 2002
Al	$Al(OH)_2^+$/$Al(OH)_3^0$/$Al(OH)_4^-$	0	Byrne 2002
V	$VO_2(OH)_2^-$/$VO_3(OH)^{2-}$/VO_4^{3-}	−	Byrne 2002
Cr	$Cr(OH)_2^+$, $Cr(OH)_3^0$, $Cr(OH)_4^-$	0	Byrne 2002
Mn	Mn^{2+}(72%), $MnCl^+$(21%)	+	Byrne 2002
Cu	Cu^{2+}/$CuOH^+$, Cu^{2+}/$CuCO_3^0$	+	Byrne 2002
Zn	Zn^{2+}(64%), $ZnCl^+$(16%)	+	Byrne 2002
Ga	$Ga(OH)_2^+$/$Ga(OH)_3^0$/$Ga(OH)_4^-$	0	Byrne 2002
As	$H_2AsO_4^-$/$HAsO_4^{2-}$/AsO_4^{3-}; $As(OH)_3^0$/$As(OH)_4^-$	−	Byrne 2002
Rb	Rb^+(99%), $RbSO_4^-$(1%)	+	Byrne 2002
Mo	$HMoO_4^-$/MoO_4^{2-}	−	Byrne 2002
Ag	$AgCl_3^{2-}$(66%), $AgCl^{2-}$(26%)	−	Byrne 2002
Cd	$CdCl^+$(36%), $CdCl_2^0$(45%), $CdCl_3^-$(16%)	+	Byrne 2002
Sb	$Sb(OH)_5^0$/$Sb(OH)_6^-$	−	Byrne 2002
Cs	Cs^+(99%)	+	Byrne 2002
Ba	Ba^{2+}(86%), $BaSO_4^0$(14%)	+	Byrne 2002
W	HWO_4^-/WO_4^{2-}	−	Byrne 2002
U	$UO_2(CO3)_3^{4-}$	−	Endrizzi & Rao 2014

Table 2.5 Relative abundance of dissolved inorganic species in seawater. Li, Mn, Cu, Zn, Rb, Cd, Cs and Ba mainly exist as free cations or positively charged complexes in seawater, (Byrne 2002) whereas V, As, Mo, Ag, Sb, W and U exist in seawater as negatively charged ions (Byrne 2002; Endrizzi and Rao 2014).

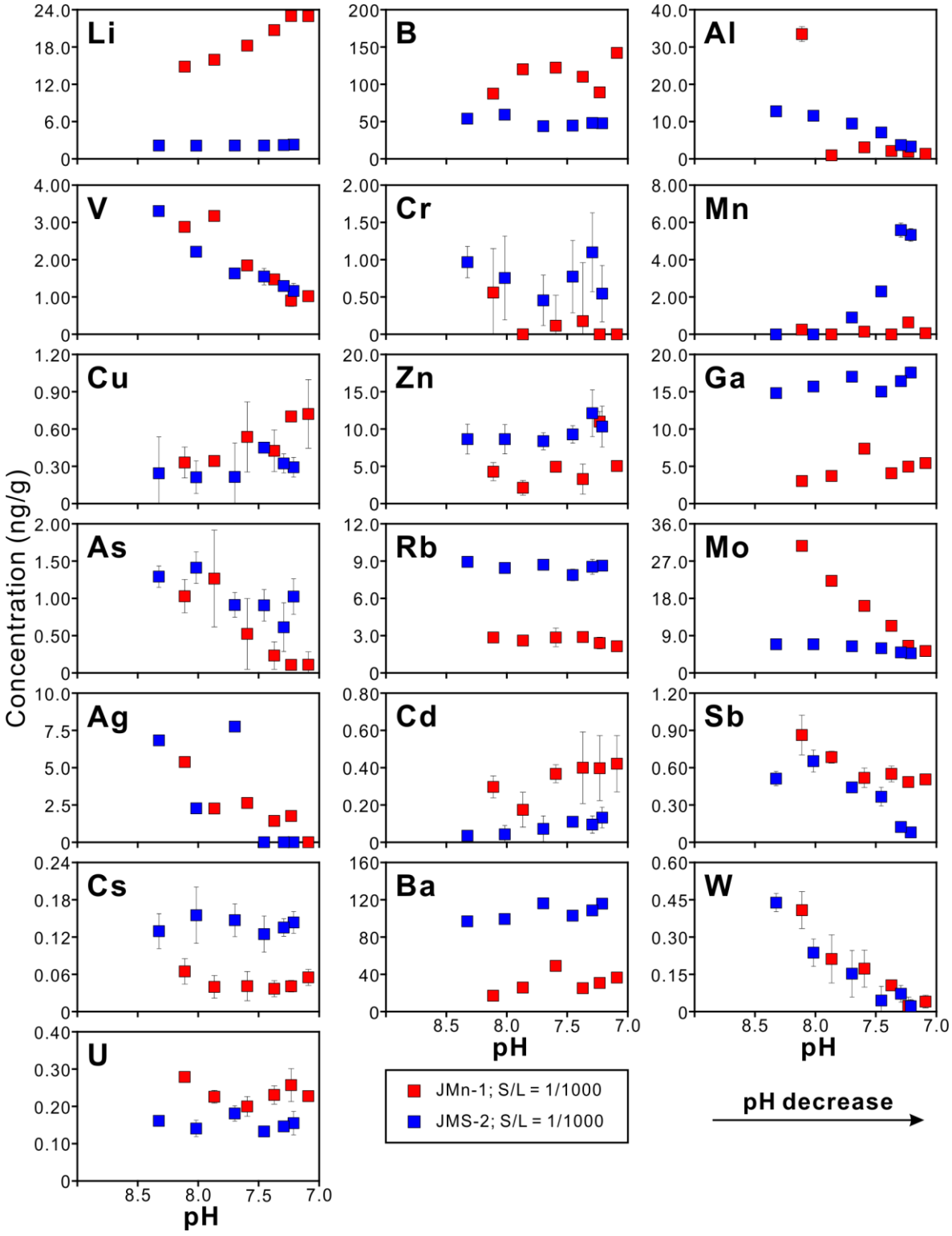

Figure 2.4 Element concentrations in the filtrate ASW sample in response to pH after 24 hours exposure of the JMn-1 and JMS-2 to ASW (S/L(solid-to-liquid) =1/1000).

ASW increased, almost no Mn was released from Fe–Mn nodules; therefore, Mn concentrations in the ASW (JMn-1) shown no significant variation. The Mn concentration in the ASW (JMS-2) shown a distinct increase as pH of the seawater decreased, which may suggest that the amount of Mn in exchangeable fraction of pelagic clays is higher than that in exchangeable fraction of Fe–Mn nodules. The different trend of element concentration observed for Li and Mo in JMn-1 trials and JMS-2 trials may be attributed to the same reason. Comparing to the ASW (JMn-1), low element concentration of Li and Mo in ASW (JMS-2) suggests that the amount of Li and Mo in the exchangeable fraction of JMS-2 is lower than that in JMn-1, therefore, as the pH of ASW samples decreases, the amplitude of Li and Mo in ASW (JMS-2) is much smaller than that in ASW (JMn-1).

4.5. Influence of pH change on deep-sea Fe–Mn nodules and pelagic clays

The pH of seawater varies both spatially (from the deep-sea to shallow sea) and temporally (from present to the coming centuries); therefore, an assessment of metal release from deep-sea sediments should be taken into consideration. To assess the influence of pH changes on deep-sea Fe–Mn nodules and pelagic clays (in this study, JMn-1 and JMS-2), the concentrations of B, Al, Cr, Mn, Cu, Zn, As, Mo, Ag, Cd, Sb, Ba, W and U used in the study were compared with the chemical composition of natural seawater (Yuan-Hui 1991) and there widely used international water quality criteria: EC (European Communities) 1998; WHO (World Health Organization) 2011; USEPA (United States Environmental Protection Agency)

2012. Depending on the S/L ratio, a certain factor must be multiplied to the concentration of elements in leachates before they can be compared with the water quality standard (Gupta, et al. 2005; WHO 2011; USEPA 2012). Previous studies used a factor of 0.1 when using a S/L ratio of 1/10 and 1 with a S/L ratio of 1/100. The S/L ratio used here was 1/1000; therefore, a factor of 10 should be multiplied to the element concentration in ASW (Figure 2.5).

Comparing the results of this study with the water quality criteria, Al, Cr, Mn, Cu, Zn, Sb and U were generally below their threshold limits for water quality criteria. However, when comparing with the strictest criterion, Al concentration in ASW samples treated with pelagic clay (JMS-2) exceeded its criterion when the pH was higher than 7.46. When the pH dropped lower than 7.46, the Mn concentration in ASW samples treated with pelagic clay (JMS-2) exceeded its threshold. The concentration of As in the JMn-1 and JMS-2 trials exceeds the criteria when pH values were higher than 7.87. Furthermore, the concentration of Mo in all samples exceeded the WHO criterion, although it did show good linear variation with decreasing pH. Cd concentration was harmful according to the strictest criterion in the ASW samples treated with JMn-1 with a pH lower than 7.60. Contrarily, samples with pH values higher than 7.37 shown a slight desorption of Sb.

The concentration of almost all elements in the ASW samples exceeded that of natural seawater, except for Uranium (Figure 2.5). Concentrations of heavy metals Mn, Cu, Zn and Cd increased as the pH decreased and exceeded that of natural seawater by a factor of 10–740, 10–35, 60–340 and 10–50, respectively. The concentration of toxic elements, such as As

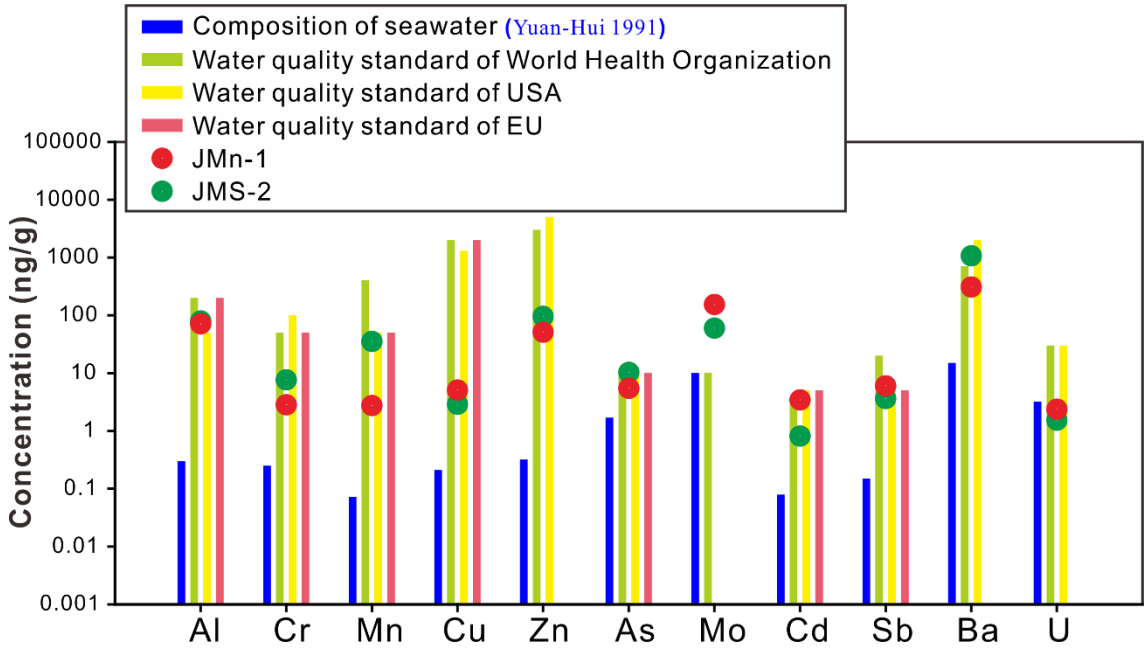

Figure 2.5 Comparison of dissolved multi-elemental concentrations in ASW measured with S/L (solid-to-liquid) = 1/1000 experiments at different pH with those of natural seawater and those indicated in international water quality criteria. (Data in this figure are multiplied by a factor of 10; see the text)

and Ag, also exceeded that of natural seawater, but these elements tended to be released at weak alkaline conditions rather than at low pH.

4.6. Comparison with sediment-seawater interaction in natural aquatic environments

Differences and similarities between seawater in natural aquatic environments and ASW used in this study need to be carefully considered when comparing our results with those from natural aquatic environments. The temperature used in this study is close to that in sea surface environment. The result provides a good assessment when fine particles of Fe–Mn nodule and pelagic clays are brought to the sea surface by deep-sea mining operations. However, this temperature is much higher than that of the deep-sea waters, directly transposing the result to the deep-sea may lead to an overestimate of the mobilities of the elements. Our result shown that some elements in ASW samples exceeds the water quality criteria and even almost all elements exceeded the composition of natural seawater, but considering the overestimate caused by higher temperature, the release of elements from sediments into seawaters occurring in deep-sea might be less. Furthermore, the geochemical reference samples, JMn-1 and JMS-2, used in our experiments had been crushed into fine pieces during the preparation of the geochemical reference materials by the Geological Survey of Japan (Terashima et al., 1995; Terashima et al., 2002). This may bring about differences between in-situ processes and in-door experiments in terms of the particle size of the Fe–Mn nodules and pelagic clays. Deep-sea mining operations are expected to resuspend

huge amounts of sediment into the water column (Glasby, 2006; Kim et al., 2013; Sharma, 2015), released tailings and uncontrolled discharge accompanied by pipe breakage (Oebius et al., 2001). In our experiments, the fresh surface of finely-crushed samples was directly exposed to ASW, which provides a good analog for resuspended sediment or released tailings, where the fine particles are directly exposes to the seawater. In addition, to minimize biological effects and to provide reproducible solutions of known composition, ASW without organic components was produced in this study, but natural seawater has a certain level of organic components (Senanayake 2011).

Despite the above differences, the usage of ASW and CO_2-induced pH regulation system allowed us to investigate the element behavior in response to the seawater pH changes caused by ocean acidification and to estimate potential element release from two representative metal rich deep-sea sediments under the background of ocean acidification. The release of elements those exist as positively charged ions becomes easier when seawaters become more acidified, this trend is not affected by temperature or sediment-to-seawater ratio. Therefore, the release of this type of elements, such as Mn, Cu, Zn and Cd, should be taken into consideration when assessing the potential influence of ocean acidification on deep-sea Fe–Mn nodules and pelagic clays.

5. Conclusions

The pH drifting observed is consistent with the pH regulating processes caused by reactions between surface hydroxyl groups on solid phase and charged ions/complexes in the ASW. Based on the pH changes, the pH_{PZC} values of JMn-1 and JMS-2 in the ASW is estimated to be ~7.4 and ~7.7, respectively. The buffer capacities of JMn-1 and JMS-2 imply that deep-sea sediments may have local effects on pH of seawater when S/L ratio is large.

Considering the mild and narrow pH range caused by ocean acidification, elements those can release into seawater should be mainly derived from the exchangeable fractions of Fe–Mn nodules and pelagic clays. Variations in the concentrations of elements are affected by sorption-desorption processes, which are primarily determined by changes in the pH-regulated surface charge of solid phase and the ion species in seawater.

Decreasing pH of ASW enhanced the release of elements taking positively charged species, although these concentrations did not far exceed the water quality criteria. In terms of the potential risk of heavy metal release, Mn, Cu, Zn and Cd should be taken into consideration when assessing the influence of ocean acidification on deep-sea environment.

Chapter 3

Response of planktonic foraminiferal shells to ocean acidification revealed by X-ray microcomputed tomography

Abstract

In this chapter, the size-normalized weight of *Globigerinoides ruber* (white) shells in core MD98-2196 was measured. The result tracks the variation of atmospheric pCO_2 and confirms the previous studies those arguing the size-normalized weight reflects surface seawater carbonate chemistry. The clean surfaces, unambiguous silhouette, and well-preserved pores on the outer shells of *G. ruber* (w) revealed by the high-resolution X-ray microcomputed tomography (XMCT) images indicate that the shells of *G. ruber* (w) in all the core samples suffered from almost negligible post-depositional alteration. The XMCT-derived foraminiferal shell volume and shell density improved our understanding of the representative meaning of the foraminiferal size-normalized weight. Ocean acidification affects the shell volume (i.e., shell wall thickness) rather than shell density of foraminiferas. This result is new direct evidence supporting previous studies. The result indicates that increasing atmospheric pCO_2 associated with ocean acidification will hinder the foraminiferas to secrete thick carbonate shells, this may have a significant influence on paleoceanographic applications of the planktonic foraminiferal shell.

1. Introduction

Absorption of atmospheric CO_2 into the oceans regulates the CO_2 partial pressure (pCO_2) in the atmosphere, alters the acidity of the surface seawaters; meanwhile, changes surface seawater carbonate ion concentration [CO_3^{2-}]. Since the pre-industrial era, the oceans have taken up approximately 50% of the anthropogenic CO_2, lowering the pH of the surface seawaters, known as "ocean acidification". The process of ocean acidification has been demonstrated from a series of simulations, hydrographic surveys, and time series data (Caldeira and Wickett 2003, Key et al. 2004, Raven et al. 2005, Kump et al. 2009).

Although the absorption of atmospheric CO_2 by the seawaters mitigates pCO_2 rise, oceanic uptake has caused a decline of surface seawater [CO_3^{2-}] and in turn a decrease in calcite and aragonite saturation states. By the middle of this century, an increased atmospheric pCO_2 will decrease the carbonate saturation state in the tropics by 30% relative to the pre-industrial values (Kleypas et al. 1999).

Many marine organisms, such as coral reefs, coccolithophorids, and foraminiferas build up their skeletons/shells by using carbonate ion in the ambient seawaters. Pieces of evidence show that carbonate saturation state is correlated with the rate of marine calcium carbonate production and is sensitive to elevated pCO_2 (Kleypas et al. 1999, Riebesell et al. 2000, Barker and Elderfield 2002, Orr et al. 2005, Raven et al. 2005, Ridgwell and Zeebe 2005, Moy et al. 2009). Foraminiferas are among the most abundant testate protists in the world's ocean, and their shells make up a significant portion of the inorganic carbon deposit on the

seafloor (Langer 2008). Planktonic foraminifera shells transfer and deposit about 32–80% of the total calcium carbonate ($CaCO_3$) preserved in deep-sea surface sediments (Schiebel 2002). A variation in calcification rate of planktonic foraminifera shells may have a significant impact on the global carbon cycle. On the other hand, metrics of planktonic foraminiferal calcification rate have been proposed to be used as potential proxies for changes in marine carbonate chemistry (Barker and Elderfield 2002, Moy et al. 2009, Marshall et al. 2013). Consequently, it is imperative to understand how and the extent to which the ocean acidification affects the calcification of planktonic foraminifera by decreasing surface seawater [CO_3^{2-}].

Initial observation of carbon and oxygen isotopic covariation in response to changing [CO_3^{2-}] invoked much attention on the relationship between foraminiferal calcification rate and ambient [CO_3^{2-}] (Spero et al. 1997, Bijma et al. 1999). The size-normalized weight has been employed as a proxy for the calcification of foraminiferal shells ever since Barker and Elderfield (2002) reported a strong positive linear correlation between ambient [CO_3^{2-}] and planktonic foraminiferal size-normalized weight. Thereafter, the size-normalized weight of foraminiferas has been used to reflect the surface carbonate system (Bijma et al. 2002, Mekik and Raterink 2008, Moy et al. 2009, Naik et al. 2010, Marshall et al. 2013, Marshall et al. 2015, Osborne et al. 2016). However, some studies suggested that other environmental variables such as optimum growth conditions and carbonate saturation state of the bottom waters may also affect the size-normalized weight of foraminiferal shells. The temperature

of seawater has been considered as a control on the size variation of foraminiferal shells, with warmer seawater producing larger and heavier shells (Bé et al. 1973, Schmidt et al. 2004, Lombard et al. 2009, Hemleben et al. 2012). Implicitly assuming the surface carbonate system has little effect on foraminiferal calcification, foraminiferal shell weight has been used as a tracer of the carbonate saturation state of the bottom waters (Lohmann 1995, Broecker and Clark 2001). Since conflicting results have emerged addressing the reliability of size-normalized weight as a proxy for surface seawater [CO_3^{2-}], it is urgent to attain a better understanding of the relationship between foraminiferal shell calcification rate and surface seawater [CO_3^{2-}].

Foraminiferal culture experiments have been used as a handy and efficient way to estimate the effects of environmental variables such as temperature and [CO_3^{2-}] since these variables can be designedly controlled in the experiments. A couple of culture studies have shown that a decrease in [CO_3^{2-}] resulted in decreased foraminiferal calcification rate for various foraminiferal species (Spero et al. 1997, Bijma et al. 1999, Bijma et al. 2002, Russell et al. 2004, Lombard et al. 2010, Manno et al. 2012). However, comparing to the result of culture experiments, studies on marine sediment samples (plankton tow samples, sediment trap samples, and core samples) have shown an even stronger influence of seawater [CO_3^{2-}] on foraminiferal calcification rate (Naik and Naidu 2007, Gonzalez-Mora et al. 2008, Mekik and Raterink 2008, de Moel et al. 2009, Moy et al. 2009, Beer et al. 2010a, Aldridge et al. 2012, Marshall et al. 2013, Osborne et al. 2016). The difference between culture experiments

and marine sediment sample studies is imputed to that the cultured foraminifera did not complete their entire life cycle under the culture experiment conditions (Bijma et al. 2002). It infers that the usage of marine sediment samples and selecting the individuals that have completed the entire life cycle will provide a better estimate of the relationship between foraminiferal shell calcification rate and surface seawater [CO_3^{2-}]. Whereas, in the case of using marine sediment samples, the post-depositional alteration such as bottom water dissolution and secondary calcite precipitation on the foraminiferal shells may confuse the application of size-normalized weight for reflecting surface seawater [CO_3^{2-}] (Marshall et al. 2013, Osborne et al. 2016). A thoroughly examining of the post-depositional alteration is essential before estimating the relationship between foraminiferal shell calcification rate and surface seawater [CO_3^{2-}] by using size-normalized weight.

Recent advances in X-ray microcomputed tomography (XMCT) has provided a novel approach to observe the internal ultra-structures of foraminiferal shells (Johnstone et al. 2010, Görög et al. 2012, Iwasaki et al. 2015). Due to its μm level high-resolution and three-dimensional (3-D) scanning capacity, XMCT measurement of foraminiferal shells enables us to obtain datasets of shell mass, density, volume, surface area, and diameter of foraminifera individuals (Iwasaki et al. 2015, Iwasaki et al. 2018). Furthermore, the internal ultra-structure and density distribution of the foraminiferal shells revealed by XMCT fill the role in estimating the bottom water dissolution (Johnstone et al. 2010, Iwasaki et al. 2015) and secondary calcite precipitation (Kontakiotis et al. 2017) of the shells. In this study, *G. ruber*

(w) individuals were picked from core samples collected from the East China Sea. Comparing the XMCT results of *G. ruber* (w) with the previously reconstructed sea surface temperature (SST) and the atmospheric pCO_2, we investigate the response of *G. ruber* (w) shells to ocean acidification during the past 100,000 years.

2. Materials and Methods

2.1. Sample selection

Foraminiferal shells collected from sediments under the lysocline may have suffered from deep water dissolution due to the undersaturation in respect to calcite. Therefore, it is essential to select sediments from the area above lysocline. The piston core MD98-2196 used in this study was collected during IMAGES-IV cruise (1998). The core is located on the seafloor of the Okinawa Trough, East China Sea (29°52.58′N, 128°36.50′E) (Figure 3.1), with a water depth of 951 m. This water depth shallower than the depth of the lysocline (2,300–3,000m) in the equatorial Pacific (Pälike et al. 2012).

The core has a total length of 3888 cm and is generally composed of homogeneous clay to silty clay, interrupted by 12 tephra layers and four fine silt layers (Ujiié and Ujiié 2006). The stratigraphy of the core was established based on the stable oxygen isotope ratios ($\delta^{18}O$) of the planktonic foraminifera *Globigerinoides sacculifer* (Ujiié and Ujiié 2006). The chronology was obtained by graphic correlation to the reference curve LR04 (Lisiecki and Raymo 2005) and accelerator mass spectrometer (AMS) ^{14}C ages. The AMS ^{14}C ages analysis

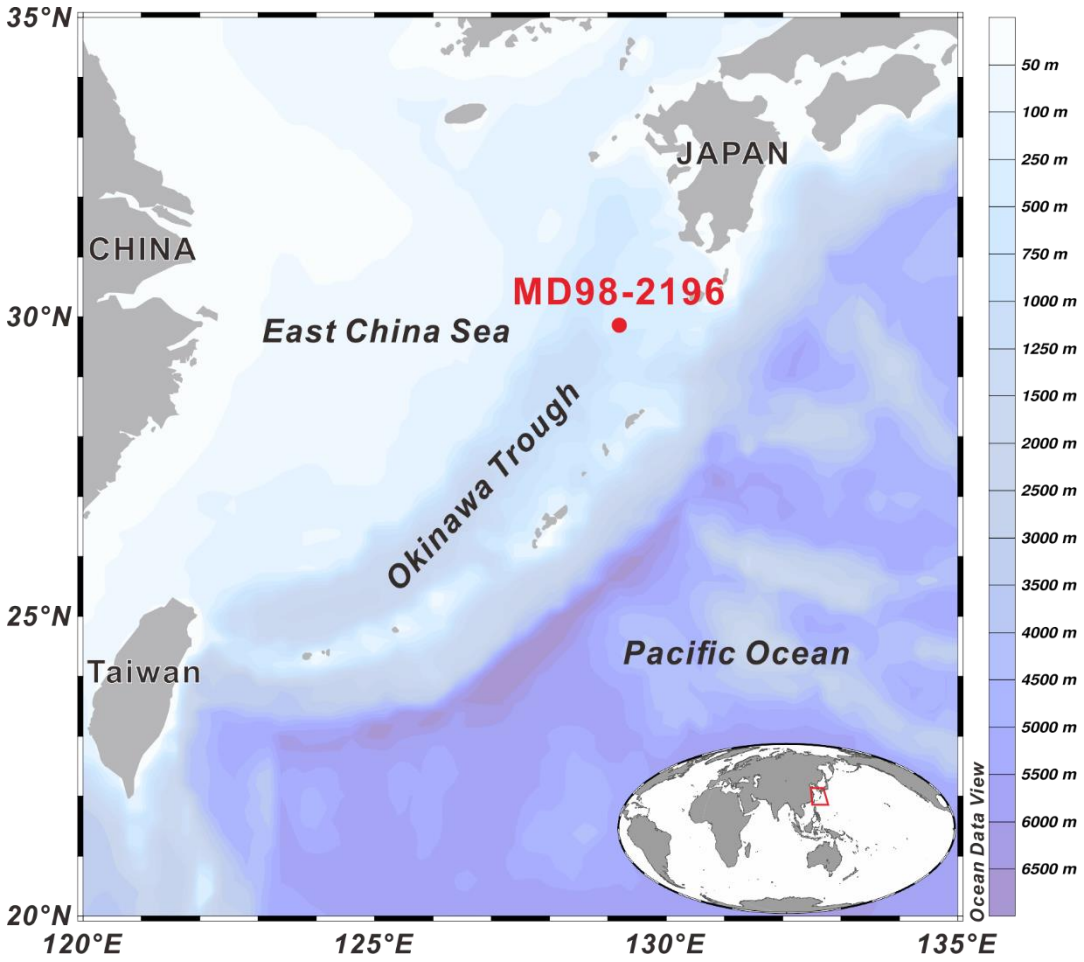

Figure 3.1 Core location. The core MD98-2196 was collected from the Okinawa Trough, East China Sea (29°52.58′N, 128°36.50′E). The water depth is 951 m, which is shallower than the present depth of the lysocline (2,300–3,000m) in the equatorial Pacific.

were performed on planktonic foraminiferal shells of *Neogloboquadrina dutertrei* from two samples (depth in core: 0 and 92 cm) and were converted into calendar ages by using the MARINE13 calibration curve in the CALIB 7 radiocarbon calibration program (Reimer et al. 2013) without ΔR correction. Core MD98-2196 covers a time interval over the last 190 kyr, from the end of marine isotope stage (MIS) 7 to the Holocene. The average sedimentation rates were 30.4 cm/kyr during glacial periods and 16.9 cm/kyr during interglacial periods (Ujiié et al. 2016). To cover the variation range of pCO_2, [CO_3^{2-}], and pH over the last 100,000 years, we selected six samples from the core MD98-2196. The samples are listed in Table 3.1.

Age (kyr)	Atmospheric pCO_2 (ppmv) [1]	Mg/Ca-derived SST (°C) [2]
3	278.8	26.4
10	262.1	24.0
20	189.2	20.3
70	213.7	23.2
90	212.0	23.8
100	231.7	24.8

[1] Petit et al. 1999
[2] Ujiié et al. 2016

Table 3.1 List of the selected samples and the reconstructed SST and atmospheric pCO_2.

2.2. Foraminifera collection and weight-size measurement

The foraminiferal calcite shells are sensitive to acid. The usage of acidic chemical reagents during sample pre-treatment may bring significant bias in the measurements of shell

weights and shell volume. Before the experiment, we conducted a couple of testing experiment to confirm the cleaning procedure. Finally, we found that carefully conducted water flush washing is adequate to remove the clays or coarse-grained silicates. 5~8 cm^3 of sediment samples were dried under 40°C for 12 hours and then washed and sieved through a 63 μm mesh. All the shells of *G. ruber* (w) were picked from the samples (300–480 μm size fraction) under a stereomicroscope (Olympus SZX12, Olympus Optical Co., Ltd., Tokyo, Japan).

The weights of individual shells were measured with a microbalance (Orion Cahn C-35 Thermo Scientific, USA). Analytical precision during the weight measurements was 0.4 μg (±1σ) (n=20). Individual foraminiferal shells from each sample were photographed with the stereomicroscope for size analysis (Figure 3.2). Digital images of all shells were taken with a digital microscope camera (Olympus E-PL6, Olympus Optical Co., Ltd., Tokyo, Japan), and the sizes of the shells were determined with graphics process software (CorelDRAW X8, Corel Co. Ltd. USA).

Due to that, the XMCT measurement is quite time consuming, XMCT measurements were not performed on all foraminifera individuals. Instead, 3~6 foraminifera individuals which have the size-normalized weight value that close to the mean value were selected for XMCT measurements.

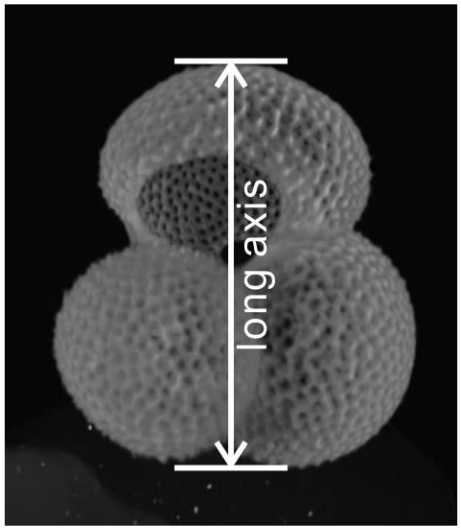

Figure 3.2 Shell of *G. ruber* (w) for size measurement. The length of long axis is used as the shell size.

2.3. X-ray microcomputed tomography measurement

A ZEISS Xradia 410 Versa (Carl Zeiss X-ray Microscopy, Inc., Germany) was used to image the internal ultra-structure and density distribution of the shells of *G. ruber* (w). The scanning was performed in Center for Advanced Marine Core Research, Kochi University. A high-resolution setting was used for 3-D quantitative densitometry of the foraminiferal shells (X-ray tube voltage of 80 kV and current of 125 amperes, spot pixel size of 1.0 μm, detector array size of 1,000×1,000, 3.0 second/projection and 2,100 projections/360°). The sample holder was made of a pencil core, with foraminiferal shell individuals glued on the top of the sample holder using water-soluble glue (tragacanth gum) so that the shells could be recovered afterward. A grain of quartz was mounted aside to the sample holder and scanned simultaneously with the shells to standardize the CT number of each shell. All the shells were scanned with the same quartz to calibrate the relative density of shells and to distinguish the density distributions in the foraminiferal shells with high resolution (Figure 3.3). MolcerPlus 3-D imaging software (White Rabbit Co. Ltd.) was used to process the 3-D CT image. Volume rendering was performed on a 970-tiff image stack.

2.4. Shell volume, shell wall thickness, and shell density

3-D images of each foraminiferal shell were generated based on a 970-tiff image stack and are made up as pixels. When processing the images by MolcerPlus, the 3-D image is constituted in voxels. Since the length of one side of this voxel is the resolution of XMCT

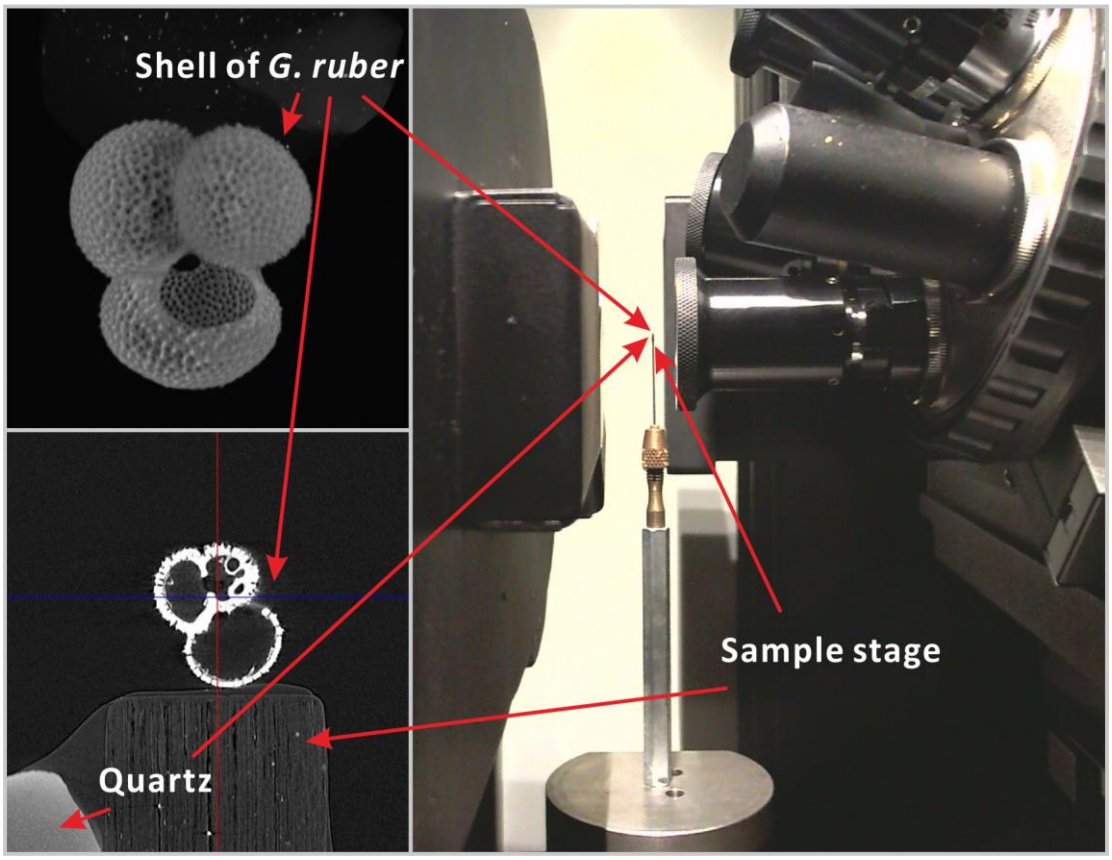

Figure 3.3 Experiment settings of the XMCT measurements. The sample holder was made of a pencil core, with foraminiferal shell individuals glued on the top of the sample holder using water-soluble glue (tragacanth gum) so that the shells could be recovered afterward. A grain of quartz was mounted aside to the sample holder and scanned simultaneously with the shells to standardize the CT number of each shell. All the shells were scanned with the same quartz to calibrate the relative density of shells and to distinguish the density distributions in the foraminiferal shells.

measurement (1.0 μm in this study), the volume of each voxel can be calculated. MolcerPlus sums up the total number of voxels of the foraminiferal shells and output their total volume as the XMCT-based shell volume of each foraminiferal shell.

Shell wall thickness is the shortest distance from the inner shell surface to the outer shell surface. Since the shell wall thickness varies from chamber to chamber (de Viler 2004), direct measurements of shell wall thickness via XMCT images cannot express the average shell wall thickness over the entire shell.

Foraminiferal shell density can be calculated in two different ways: 1) XMCT-based shell density is the value obtained directly from XMCT measurements. As described above, the 3-D image of the foraminiferal shells is constituted as voxels during data processing on MolcerPlus. The CT number of the voxels represents the density of the objects; therefore, the shell density can be calculated by averaging the CT numbers of all the voxels and normalizing the mean CT number of the shell to the CT number of the quartz which was mounted aside to the sample holder and scanned simultaneously. 2) Measure-based shell density is the value obtained by dividing the measured shell weight by the XMCT-based shell volume.

2.5. Seawater pH and [CO_3^{2-}] variation over the past 100,000 years

The atmospheric pCO_2 varied dramatically during the past 100,000 years. Since the Last Glacial Maximum (LGM), atmospheric pCO_2 had increased from about 180 ppmv to 290 ppmv (Petit et al. 1999). Accordingly, the pH and [CO_3^{2-}] of the surface seawaters should

have dropped markedly. By using the reconstructed atmospheric pCO_2 (Petit et al. 1999) and SST (Ujiié et al. 2016), and assuming the total alkalinity (TA) was constant during the past 100,000 years, the pH and $[CO_3^{2-}]$ had been calculated via CO2calc v4. We also refer to the reconstructed TA from the Caribbean Sea over the last 130 kyr (Foster 2008) to calculate the pH and $[CO_3^{2-}]$.

3. Results

Both the result of TA-constant-assuming trial and the reconstructed TA trial show that surface seawater pH and $[CO_3^{2-}]$ over the past 100,000 years reached the maximum during the LGM and dropped down rapidly thereafter (Figure 3.4). The result of shell weight and size measurements of *G. ruber* (w) in the core MD98-2196 are shown in Table 3.2, 3.3, and Figure 3.5. Shell weight values were divided by shell size to calculate the size-normalized weight. The result of the size-normalized weight, shell volume, and shell density of selected *G. ruber* (w) are shown in Table 3.4, Figure 3.5, and Figure 3.6. The size-normalized weight covaried with the concomitant atmospheric pCO_2, fluctuated from about 0.05 μg/μm to 0.02 μg/μm. The size-normalized weight of *G. ruber* (w) peaked during the Last Glacial Maximum (LGM; 18–24 kyr) and lowered during the Holocene (0–10 kyr), with about 60% decrease in size-normalized weight in response to about 30 μmol/kg-seawater increase of $[CO_3^{2-}]$ in the ambient seawater (Figure 3.4 and 3.5).

Age (ka)	3	10	20	30	40	50	60	70	80	90	100
	475	508	478	477	447	476	469	472	517	453	416
	372	423	487	430	522	489	416	506	476	379	342
	379	385	479	541	398	437	378	327	421	391	383
	456	330	398	356	383	466	403	366	449	527	337
	338	399	328	428	433	411	270	369	358	321	365
	401	443	342	352	471	489	338	321	361	397	358
	331	466	363	354	481	501	304	381	342	506	499
	341	439	333	399	481	382	438	413	479	404	446
	350	316	454	384	489	430	398	418	291	381	403
	342	483	361	445	407	413	320	359	454	452	310
	376	430	389	471	404	505	387	307	378	417	432
	292	471		426	406	514	424	466	344	407	386
	307	361		370	346	386	375	361	371	517	367
	321	426		409	430	399	280	417	360	395	385
	435	479		370	364	375	417	355	340	363	468
		296			416	352	376	447	438	436	409
		335			330	417	303	439	389	498	465
		327				387		330	356	419	356
		396				430			320	467	364
		414				404			416	537	481
		427				312			411	473	447
		347							415	388	381
		407								395	394

Units are in μm

Table 3.2 Result of shell size measurements of *G. ruber* (w) in the core MD98-2196

Age (ka)	3	10	20	30	40	50	60	70	80	90	100
	21	17	26	30	25	21	28	17	22	25	13
	13	14	17	24	24	25	11	19	19	14	9
	10	10	20	29	12	15	15	11	14	11	9
	24	10	19	14	24	16	17	18	13	22	9
	8	12	9	21	13	16	4	10	9	7	11
	12	11	9	10	14	21	12	6	7	13	7
	9	13	9	11	14	19	9	12	7	26	17
	14	15	11	15	20	15	22	13	19	11	13
	8	7	12	15	21	14	18	12	6	10	14
	8	21	9	23	12	20	6	10	22	13	6
	11	13	14	26	13	19	13	9	11	12	18
	5	20		26	15	20	19	20	9	13	13
	8	10		8	11	11	14	11	10	24	7
	10	15		12	18	18	6	11	12	11	11
	16	17		6	9	11	18	11	10	9	17
		10			19	12	14	14	17	19	14
		5			9	10	8	18	10	25	18
		9				11		10	10	17	8
		15				15			7	17	8
		10				12			17	25	23
		14				7			10	15	23
		14							12	12	11
		15								12	14

Units are in μg

Table 3.3 Result of shell weight measurements of *G. ruber* (w) in the core MD98-2196

Sample ID	Weight	Size	Weight/Size	XMCT-based Shell Volume	XMCT-based Shell Density	Measure-based Shell Density
	μg	μm	μg/μm	$\times 10^{-3}$ mm^3		mg/mm^3
3ka-05	8	338	0.024	4.6	1.4	1.8
3ka-09	8	350	0.022	5.0	1.3	1.6
3ka-13	8	307	0.026	4.1	1.4	1.9
10ka-03	10	385	0.026	5.6	1.4	1.8
10ka-06	11	443	0.026	7.2	1.4	1.6
10ka-07	13	466	0.028	7.2	1.4	1.8
20ka-03	20	479	0.042	10.5	1.3	1.9
20ka-04	19	398	0.047	10.0	1.4	1.9
20ka-11	14	389	0.037	7.5	1.4	1.9
70ka-03	11	327	0.032	5.3	1.4	2.0
70ka-08	13	413	0.032	7.6	1.3	1.8
70ka-15	11	355	0.032	6.0	1.4	1.9
90ka-02	14	379	0.036	7.1	1.3	1.9
90ka-06	13	397	0.032	6.6	1.4	1.9
90ka-12	13	407	0.032	6.8	1.4	1.9
90ka-19	17	467	0.037	8.4	1.3	2.0
90ka-21	15	473	0.032	7.9	1.2	1.9
90ka-23	12	395	0.031	7.2	1.3	1.7
100ka-01	13	416	0.031	7.4	1.3	1.7
100ka-04	9	337	0.026	4.5	1.4	1.9
100ka-08	13	446	0.030	8.0	1.4	1.7

Table 3.4 Result of the size-normalized weight, shell volume and shell density.

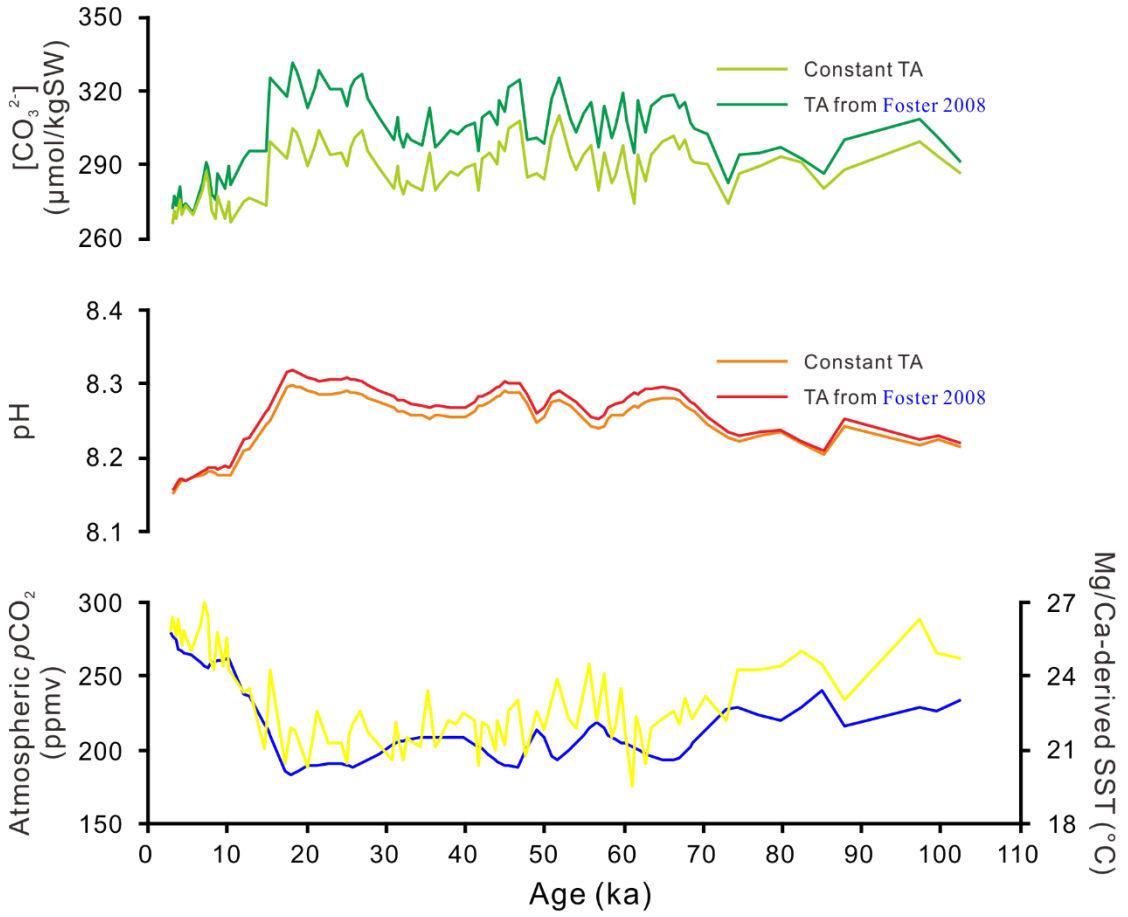

Figure 3.4 pH and $[CO_3^{2-}]$ of the surface seawater (shallower than 30m water depth) calculated by CO2calc v4.

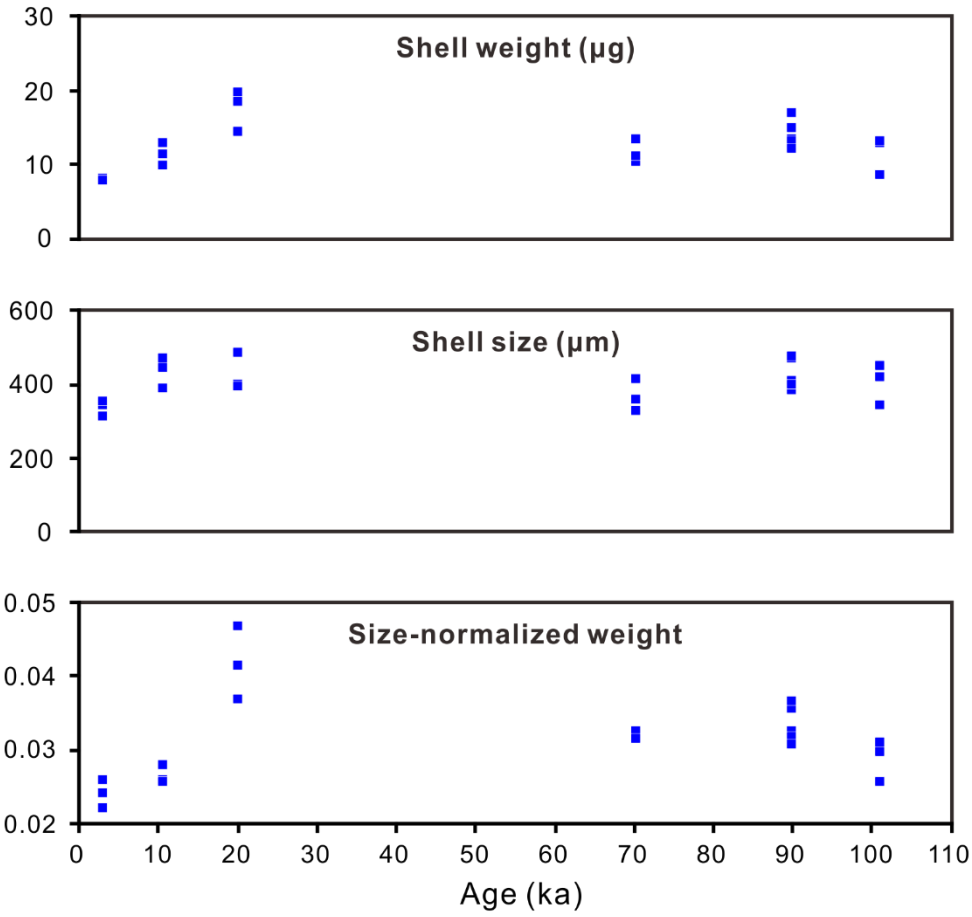

Figure 3.5 Result of shell weight and shell size measurements.

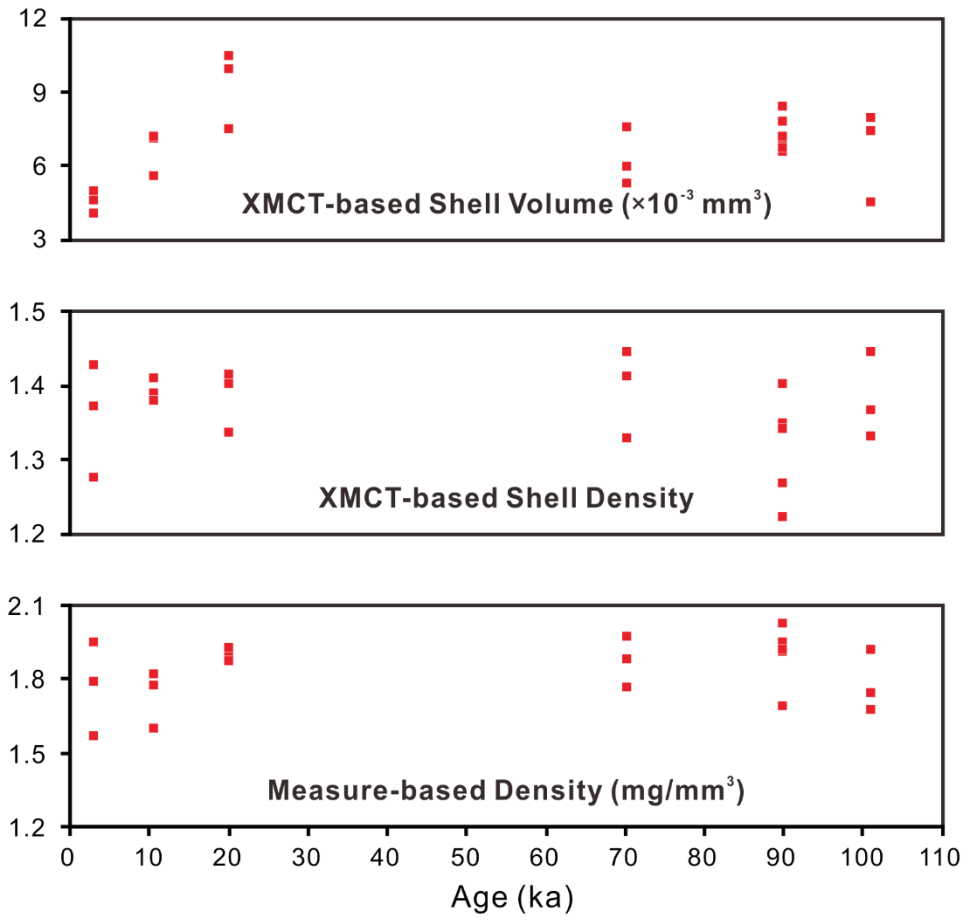

Figure 3.6 Shell volume, shell density obtained by XMCT measurements.

4. Discussions

4.1. Variables influencing the growth of planktonic foraminiferal shells

The growth of planktonic foraminifera shells has been linked not only to [CO_3^{2-}] of the surface seawater, but also to environmental variables such as seawater temperature and nutrient concentration (Bé et al. 1973; Lohmann 1995, Spero et al. 1997; Aldridge et al. 2012). The concept of "optimal growth" has been suggested to hypothesize that a combination of environmental factors controls the growth and calcification rate of planktonic foraminifera (de Villiers 2004). In this hypothesis, the calcification rate reduces when the "optimal growth" conditions are not satisfied. However, several studies attempting to verify this hypothesis did not find any influence of such "optimal growth" conditions on neither the individual calcification nor the absolute abundance of a specific species (Beer et al. 2010b, Weinkauf et al. 2013, Weinkauf et al. 2016).

The seawater temperature has been considered as a control on the size variation of foraminiferal shells, with warmer seawaters producing relatively larger shells (Bé et al. 1973, Schmidt et al. 2004, Lombard et al. 2009, Hemleben et al. 2012). de Villiers (2004) suggested that optimum temperature may play a role in foraminiferal calcification rates measured by size-normalized weight. A study of eight modern planktonic foraminifera species (*Neogloboquadrina pachyderma* (sinistral), *Neogloboquadrina pachyderma* (dextral), *Neogloboquadrina dutertrei, Globigerina bulloides, Globigerinoides ruber, Globigerinoides sacculifer, Globigerinella siphonifera* and *Orbulina universa*) found that elevated

temperature led to an increase in growth rate among all these species (Lombard et al., 2009). On the other hand, Barker and Elderfield (2002) examined the influence of temperature on the size-normalized weight of *Globigerina bulloides* by comparing foraminiferal size-normalized weight during the Last Glacial Maximum to the Holocene. Their result had shown that average size-normalized weight was higher during the Last Glacial Maximum when SST was low and [CO_3^{2-}] was high. Therefore, the authors concluded that it was [CO_3^{2-}], not temperature, dominantly influenced calcification rates of the shells. Lombard et al. (2010) observed the shell growth of *Orbulina universa* and *G. sacculifer* under different [CO_3^{2-}] with constant temperature. They found a significant increase in average shell weight with no significant change in shell size in response to elevated [CO_3^{2-}]. Another study on the growth of *Neogloboquadrina pachyderma* (sinistral) indicated that increased temperature resulted in no net change in calcification rate (Manno et al. 2012).

Although it has been suggested that temperature plays a role in the growth of foraminiferal shells, more recent advances in size-normalized weight indicated that [CO_3^{2-}] is the predominant factor controlling the calcification rate of foraminiferas (Marshall et al. 2013, Osborne et al. 2016). Since SST covaries with [CO_3^{2-}] of surface seawater, it follows that temperature sometimes cannot be invoked to explain the observed trends in size-normalized weight (de Villiers 2004).

In this present study, the size-normalized weight of *G. ruber* (w) in core MD98-2196 seemingly shown a negative correlation with SST, ($R^2 = 0.74$) (Figure 3.7). As SST rose from

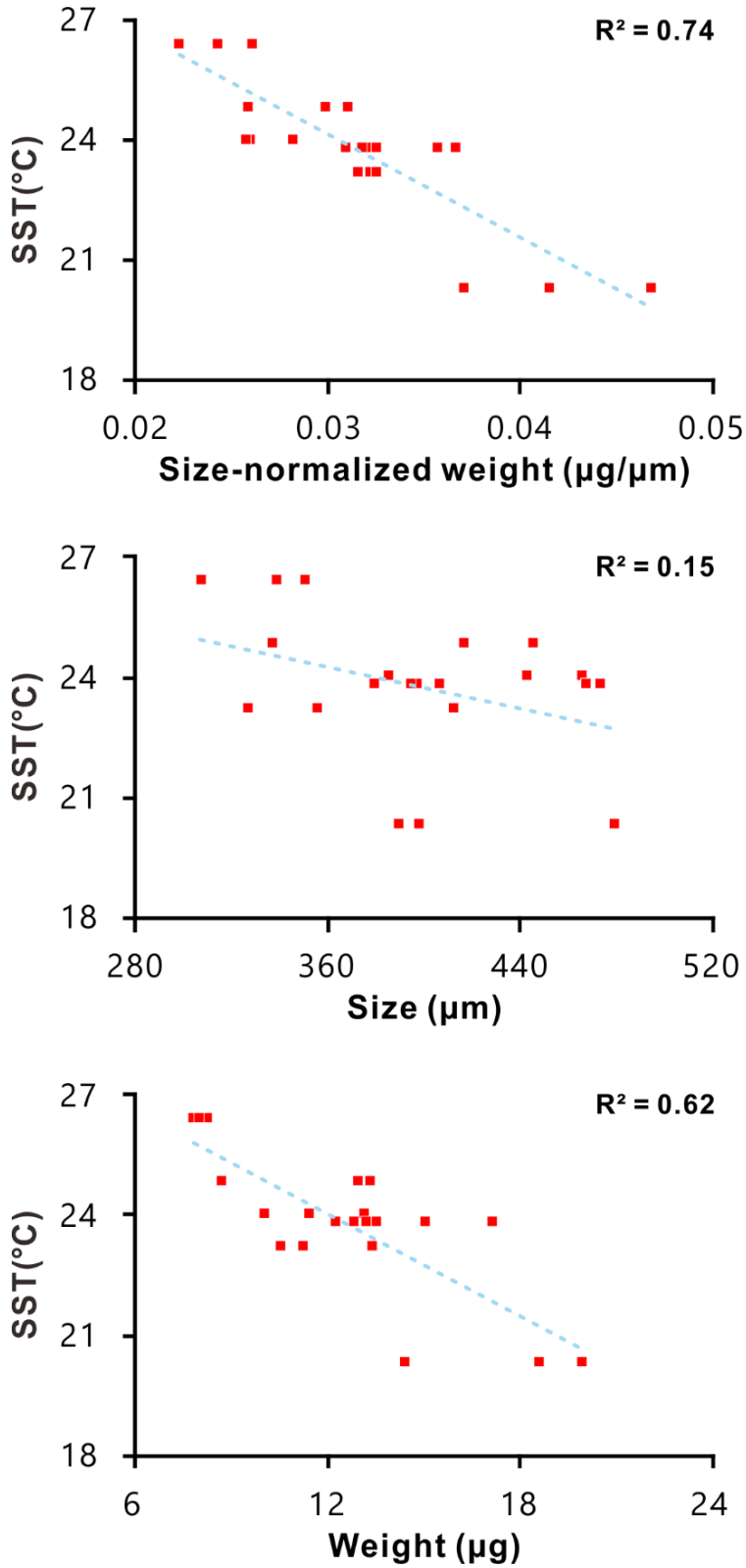

Figure 3.7 The relationship between the shell weigh, shell size and size-normalized weight of *G. ruber* (w) in the core MD98-2196 with the SST.

~19 to ~27 °C, size-normalized weight decreased from ~0.05 to ~0.02 μg/μm. However, this contradicts the optimum growth condition of this subtropical species. *G. ruber* (w) inhabits in warm subtropical surface waters, with a habitable temperature range of 14–32 °C and an optimum growth temperature of 26.5~27.0 °C (Bijma et al. 1990, Schiebel and Hemleben 2017). According to de Villiers (2004) and Bijma et al. (1990), as seawater temperature increases from ~19 to ~27 °C (close to the optimum growth temperature of *G. ruber* (w)), the growth rate or calcification intensity of the shells should be enhanced. However, our result indicated that the increased SST during the past 100,000 years have not resulted in higher size-normalized weight, which means the SST did not dominantly influence the calcification rate of *G. ruber* (w).

Some studies have suggested that nutrient concentration of the surface seawater may also affect the calcification rate of foraminiferal shells. Aldridge et al. (2012) linked the calcification rate of *Globigerina bulloides* to phosphate concentration ($[PO_4^{3-}]$) and nitrate concentration ($[NO_3^-]$) in surface waters of the North Atlantic Ocean. Based on the negative correlation between the average shell mass and the nutrient concentration, the authors inferred that a high concentration of these nutrients has adversely affected the calcification of *Globigerina bulloides*. However, the authors overlooked the strong negative correlation that exists between PO_4^{3-} and CO_3^{2-}. When $[PO_4^{3-}]$ of the surface seawater increases, $[CO_3^{2-}]$ is decreased, making it difficult to differentiate which is the best explanation of the observed variability in average shell mass of *Globigerina bulloides*. Two recent studies of sediment

trap samples in the Cariaco Basin, Venezuela, and Santa Barbara Basin, California indicated that nutrient concentration does not play a critical role in controlling calcification rate of planktonic foraminiferal species *G. ruber* and *G. sacculifer* (Marshall et al. 2013, Osborne et al. 2016). The covariation of nutrient concentration and [CO_3^{2-}] may sometimes lead to misleading correlations between the calcification rate of foraminiferal shells and the nutrient concentration in ambient seawaters (Marshall et al. 2013).

4.2. Post-depositional alteration

The extent to which the foraminiferal shells are preserved in marine sediments is another consideration for the application of size-normalized weight as a proxy reflecting surface seawater [CO_3^{2-}] (Barker et al. 2004, Gibbs et al. 2010). Below the lysocline, due to the unsaturated carbonate state of the bottom waters, the partial dissolution of planktonic foraminiferal shells may lead to underestimated size-normalized weight and bias the application of size-normalized weight as a proxy reflecting surface seawater [CO_3^{2-}]. Even above the lysocline, acidification and undersaturated carbonate states of the pore water produced by the oxidation of organic material within sediments is another significant cause of carbonate dissolution (Archer and Maier-Raimer 1994, Martin and Sayles 1996). To the opposite, in high salinity and carbonate oversaturated geological settings, the secondary calcite precipitation on the outer crust of foraminiferal shells may result in overestimated size-normalized weight by increasing the shell weight (Marshall et al. 2013). Therefore,

before being used to indicate the surface seawater carbonate chemistry, the post-depositional alteration, such as the partial dissolution or the second calcite precipitation, of the foraminiferal shells should be thoroughly examined.

Several semiquantitative methods have been developed to evaluate the post-depositional dissolution of foraminiferal shells in marine sediments. Such as the ratio of benthic to planktonic shells (Metzler et al. 1982); the ratio of unbroken to fragmentary shells (Hebbeln et al. 1990, Mekik and François 2006); the relative abundance of dissolution resistant and dissolution susceptible species (Berger 1970), and the abundance of organic linings preserved after the shell dissolved (Le and Shackleton 1992, de Vernal et al. 1992). However, since the post-depositional dissolution of foraminiferal shells initiates from the inner chambers, the observation from the outside of the shells may not be able to detect the possible post-depositional alteration (Brown and Elderfield 1996, Johnstone et al. 2010, Iwasaki et al. 2015).

A scanning electron microscopy (SEM) method has been developed to observe the potential influence of post-depositional alteration on the shells of *G. ruber* in the Eastern Mediterranean Sea (Kontakiotis et al. 2017). The high-resolution SEM images of the surface characteristic and the internal ultra-structure of *G. ruber* revealed that the shells had been profoundly affected by secondary calcite precipitation in high salinity and carbonate oversaturated situations. Johnstone et al. (2010) used an XMCT to examine the post-depositional dissolution of foraminiferal shells from core sediments. The authors divided the

post-depositional dissolution process into five stages based on the appearance of the XMCT images. This detailed study revealed that dissolution initiated from the inner chambers of the shell.

In the present study, core MD98-2196 was collected from the Okinawa Trough, East China Sea with a water depth of 951 m. This depth is shallower than the present depth of the lysocline (Pälike et al. 2012). Therefore, we infer that the post-depositional dissolution on the shells of *G. ruber* (w) in the sediments should be very limited. On the other hand, the XMCT images show that the shell walls of *G. ruber* (w) in all samples have an unambiguous silhouette, and the pores on the outer wall are well preserved (Figure 3.8), which indicates that *G. ruber* (w) shells in all samples suffered from almost negligible post-depositional dissolution and are nearly perfectly preserved (Johnstone et al. 2010). Furthermore, compared to the result of Kontakiotis et al. (2017), the XMCT images of the shell surface of *G. ruber* in all samples shown quite clean surfaces (Figure 3.8), which means *G. ruber* (w) shells in core MD98-2196 suffered from almost no precipitation of secondary calcite (Kontakiotis et al. 2017). In other words, the internal ultra-structure and surface characteristic of *G. ruber* (w) shells revealed by high-resolution XMCT images infer that shells in core MD98-2196 are well preserved, and the post-depositional alteration is almost negligible.

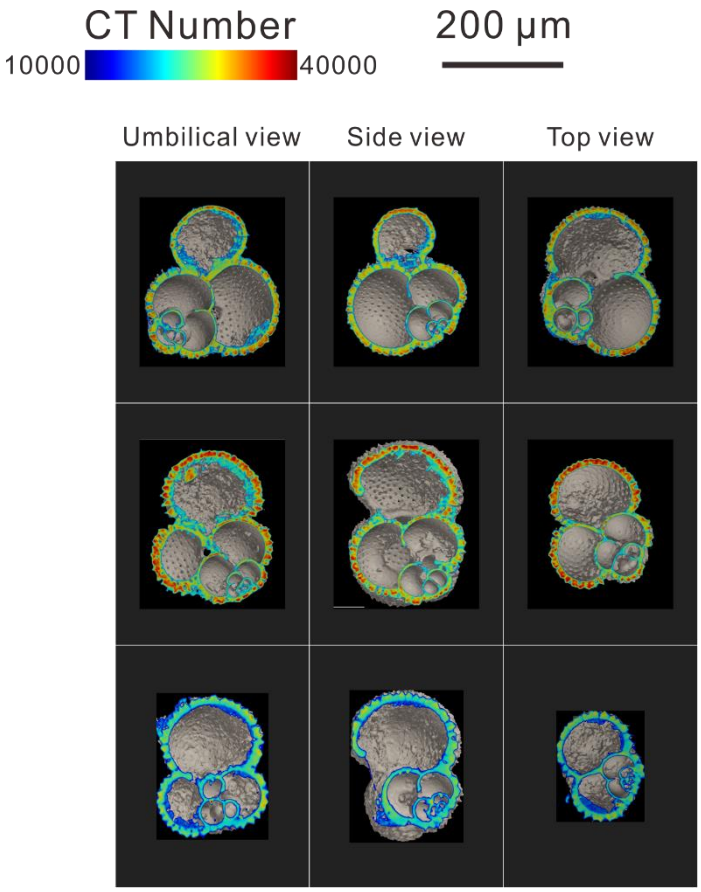

Figure 3.8 The XMCT images of the shells of *G. ruber* (w) (3ka)

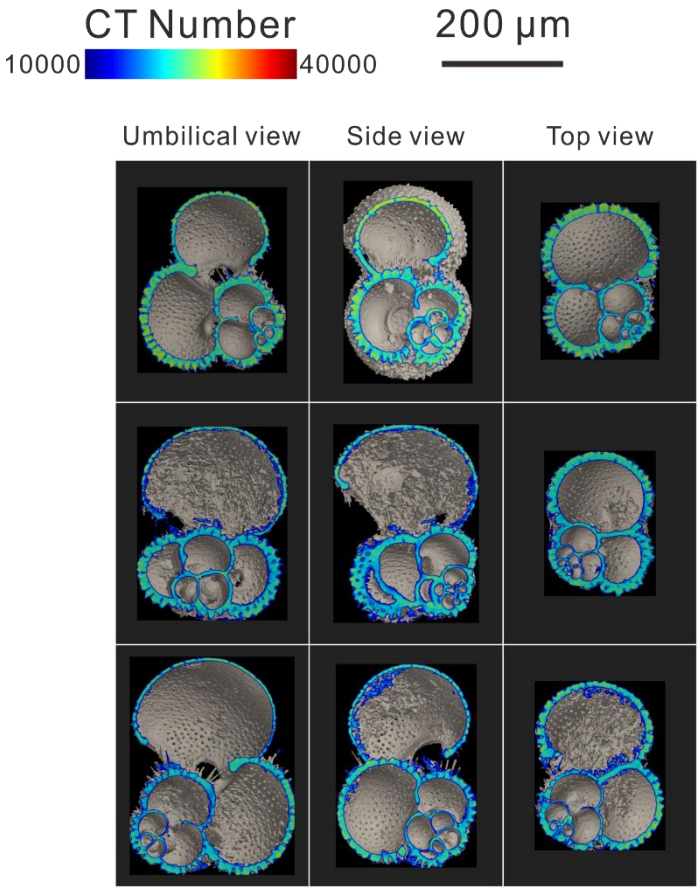

Figure 3.8 continued The XMCT images of the shells of *G. ruber* (w) (10ka).

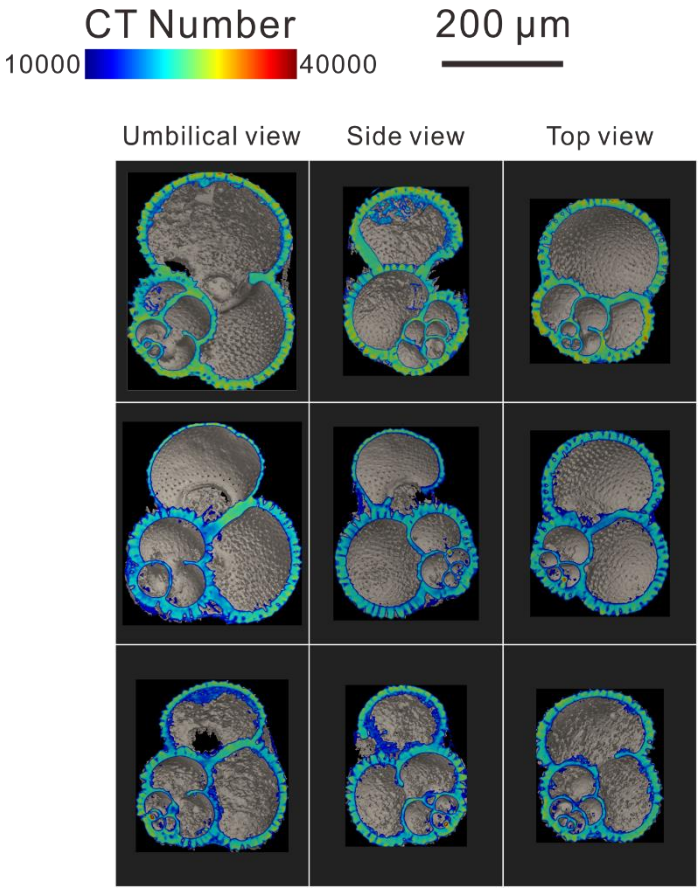

Figure 3.8 continued The XMCT images of the shells of *G. ruber* (w) (20ka).

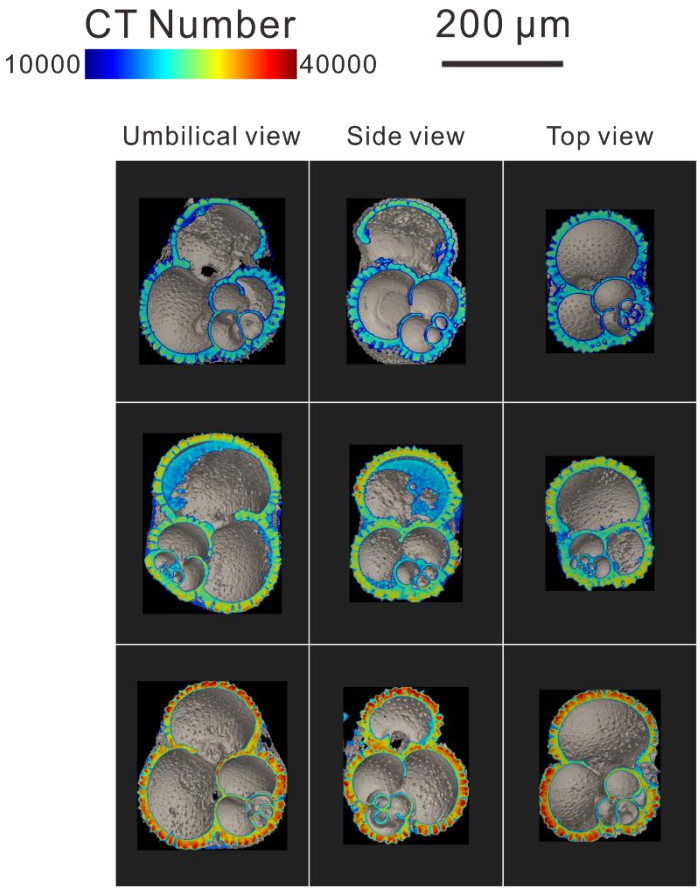

Figure 3.8 continued The XMCT images of the shells of *G. ruber* (w) (70ka).

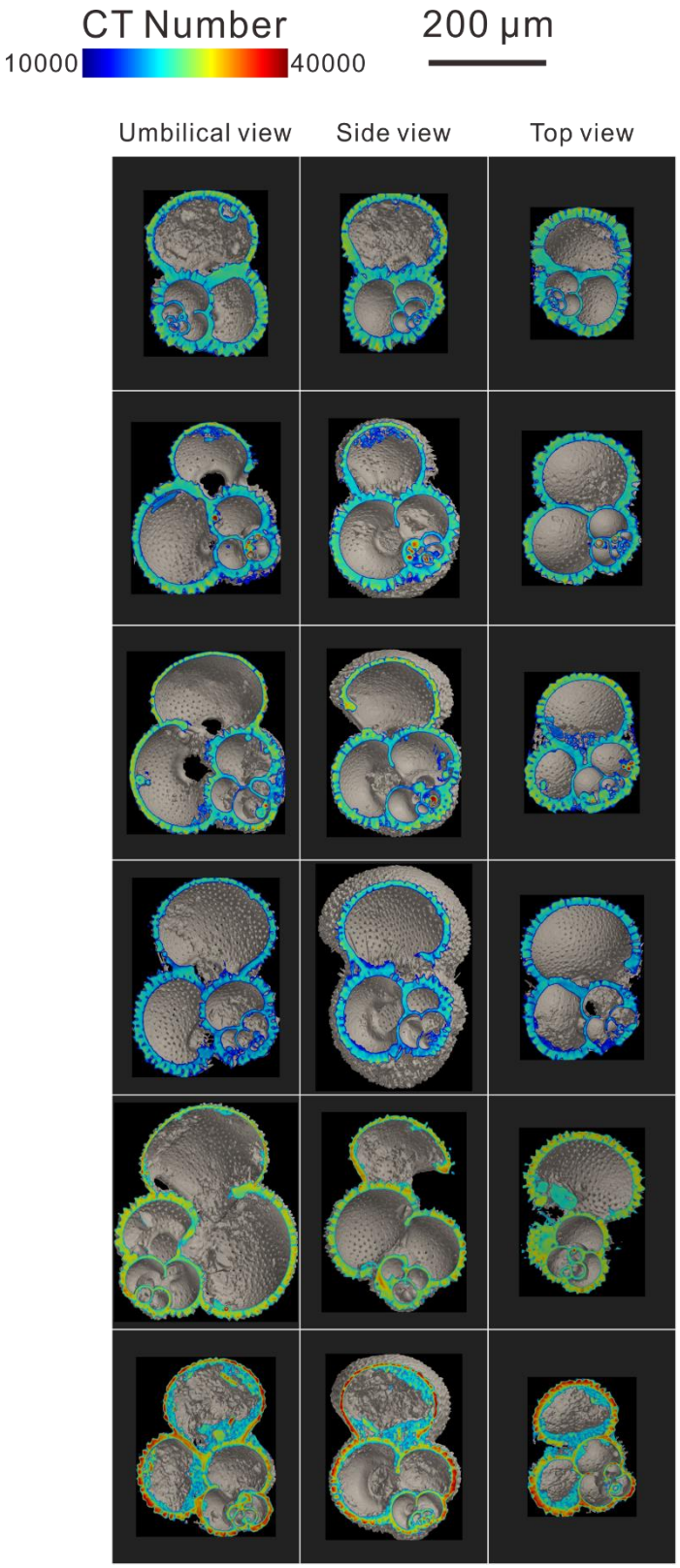

Figure 3.8 continued The XMCT images of the shells of *G. ruber* (w) (90ka).

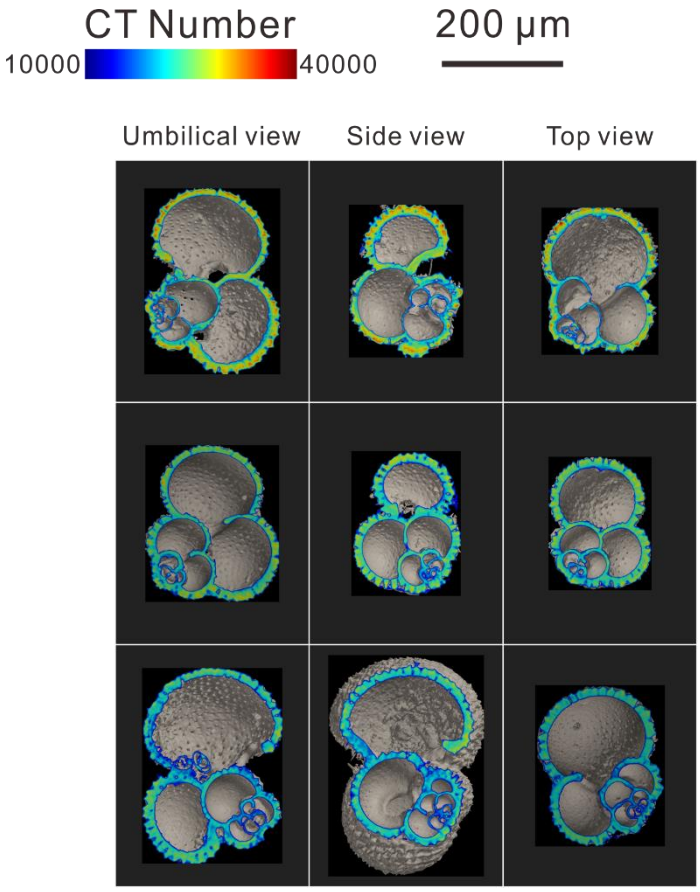

Figure 3.8 continued The XMCT images of the shells of *G. ruber* (w) (100ka).

4.3. The size-normalized weight of *G. ruber* (w) in core MD98-2196

We examined the influence of ocean acidification on planktonic foraminiferal calcification rate by comparing the size-normalized weight of *G. ruber* (w) in core MD98-2196 to the concomitant variation in seawater pH, [CO_3^{2-}], and atmospheric pCO_2 during the past 100,000 years (Figure 3.9). The atmospheric pCO_2 varied from 182 to 285 ppmv during the past 100,000 years (Petit et al. 1999). The size-normalized weight of *G. ruber* (w) in the core MD98-2196, covaried with the concomitant atmospheric pCO_2, fluctuated from about 0.05 μg/μm to 0.02 μg/μm. The size-normalized weight of *G. ruber* (w) peaked during the LGM (18–24 kyr) and lowered during the Holocene (0–10 kyr), with about 60% decrease in size-normalized weight in response to the 100 ppmv increase in atmospheric pCO_2. The observed strong correlation between the size-normalized weight of *G. ruber* (w) and the carbonate chemistry of the surface seawater agrees with previous studies (Barker and Elderfield 2002, Moy et al. 2009, Marshall et a. 2013, Osborne et al. 2016), which manifest that the size-normalized weight of planktonic foraminiferal shells primarily reflects the changes of carbonate chemistry in surface seawaters.

4.4. The representative meaning of the foraminiferal size-normalized weight

So far, the size-normalized weight of planktonic foraminiferal shells had been interpreted as either the change in shell density or the change in shell wall thickness. An essential but pendent issue is what the size-normalized weight accurately represents. The

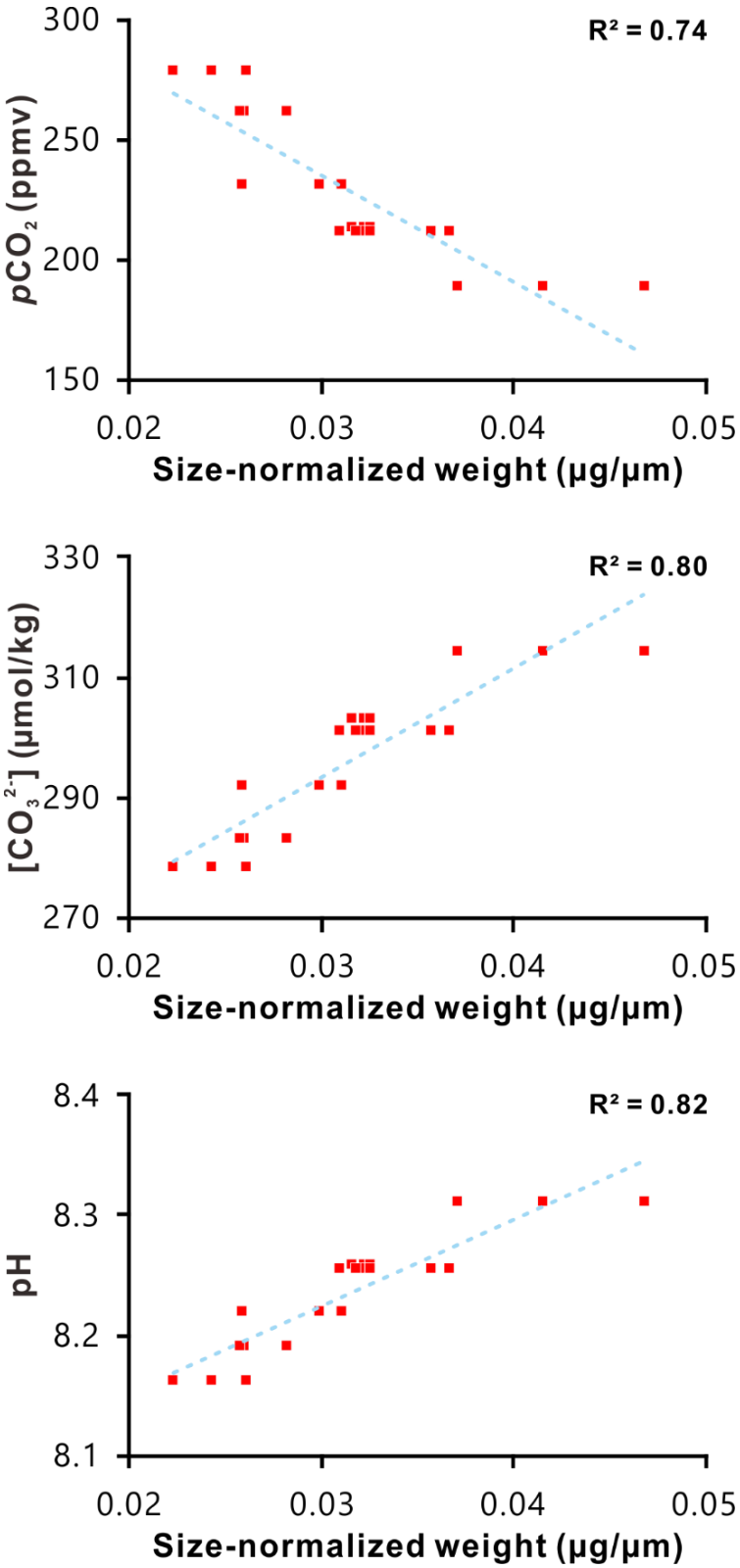

Figure 3.9 The size-normalized weight of *G. ruber* (w) in the core MD98-2196, covaried with the $[CO_3^{2-}]$ of surface seawater, fluctuated from about 0.05 µg/µm to 0.02 µg/µm.

answer to this issue may have significant implications for paleoceanographic applications of planktonic foraminiferal shell chemistry. Assuming the foraminiferal shell wall thickness is constant and does not depend on growth conditions, Broecker and Clark (2001) applied the size-normalized weight of planktonic foraminiferal shells to estimate the [CO_3^{2-}] of Atlantic upper deep water. Whereas, Bijma et al. (2002) predicted that surface seawater [CO_3^{2-}] primarily affects shell wall thickness and inferred that the size-normalized weight is a derived parameter of this relationship, however, the authors provided no direct evidence. Similarly, culture experiments of the planktonic foraminifera *Orbulina universa* have shown that an increased [CO_3^{2-}] produces higher size-normalized weights, which was implicitly interpreted as the consequence of thickened shell walls resulting from higher rates of calcification (Spero et al. 1997, Bijma et al. 1999). In another study, the observed higher foraminiferal shell weights were ambiguously attributed to denser and/or thicker shell walls (de Viler 2004). Apparently, there is no consensus yet about the issue mentioned above.

Due to the tiny size of foraminiferal shells, traditional attempts to measure the shell wall thickness and to calculate shell density will bring about significant bias. The XMCT measurements provide a novel approach to observe the internal ultra-structures of foraminiferal shells, which serves as an entrance to "read" the shell density and shell volume by CT numbers (Iwasaki et al. 2018). Based on the XMCT-derived foraminiferal shell density and shell volume datasets, we examined their relationship with the size-normalized weights. The shell density (both XMCT-based shell density and measure-based shell density) of *G.*

ruber (w) seems independent of the size-normalized weight (Figure 3.10). This is unexpected, and distinctly different from usual imagine since the size-normalized weight has by far been employed to represent the average mass over size or area and therefore reflect the surface seawater carbonate chemistry (Barker and Elderfield 2002, Moy et al. 2009, Marshall et a. 2013, Osborne et al. 2016). However, the shell density of *G. ruber* (w) and its weak correlation with size-normalized weight suggest that the foraminiferal size-normalized weight represent some other parameter rather than shell density.

Since the shell wall thickness varies from chamber to chamber (de Viler 2004), direct measurements of shell wall thickness via XMCT images cannot express the average shell wall thickness over the entire shell. As an alternative approach, we used the XMCT-based shell volume to examine the relationship between shell wall thickness and size-normalized weight (Figure 3.10). The shell volume of *G. ruber* (w) revealed by XMCT measurements shows a quite good correlation with size-normalized weight (Figure 3.10) and seawater pH, $[CO_3^{2-}]$, and atmospheric pCO_2 (Figure 3.11). It infers that the size-normalized weight of planktonic foraminiferal shells represents shell volume and in turn the shell wall thickness, and increasing atmospheric pCO_2, decreasing pH and $[CO_3^{2-}]$ associated with ocean acidification will hinder the foraminiferas to secrete thick carbonate shells. According to the result, a 100 ppmv increase in atmospheric pCO_2 may lead to about 4×10^{-3} mm^3 decreases in the shell volume of *G. ruber* (w). This result is new direct evidence supporting previous studies (Spero et al. 1997, Bijma et al. 1999, Barker and Elderfield 2002, Bijma et al. 2002).

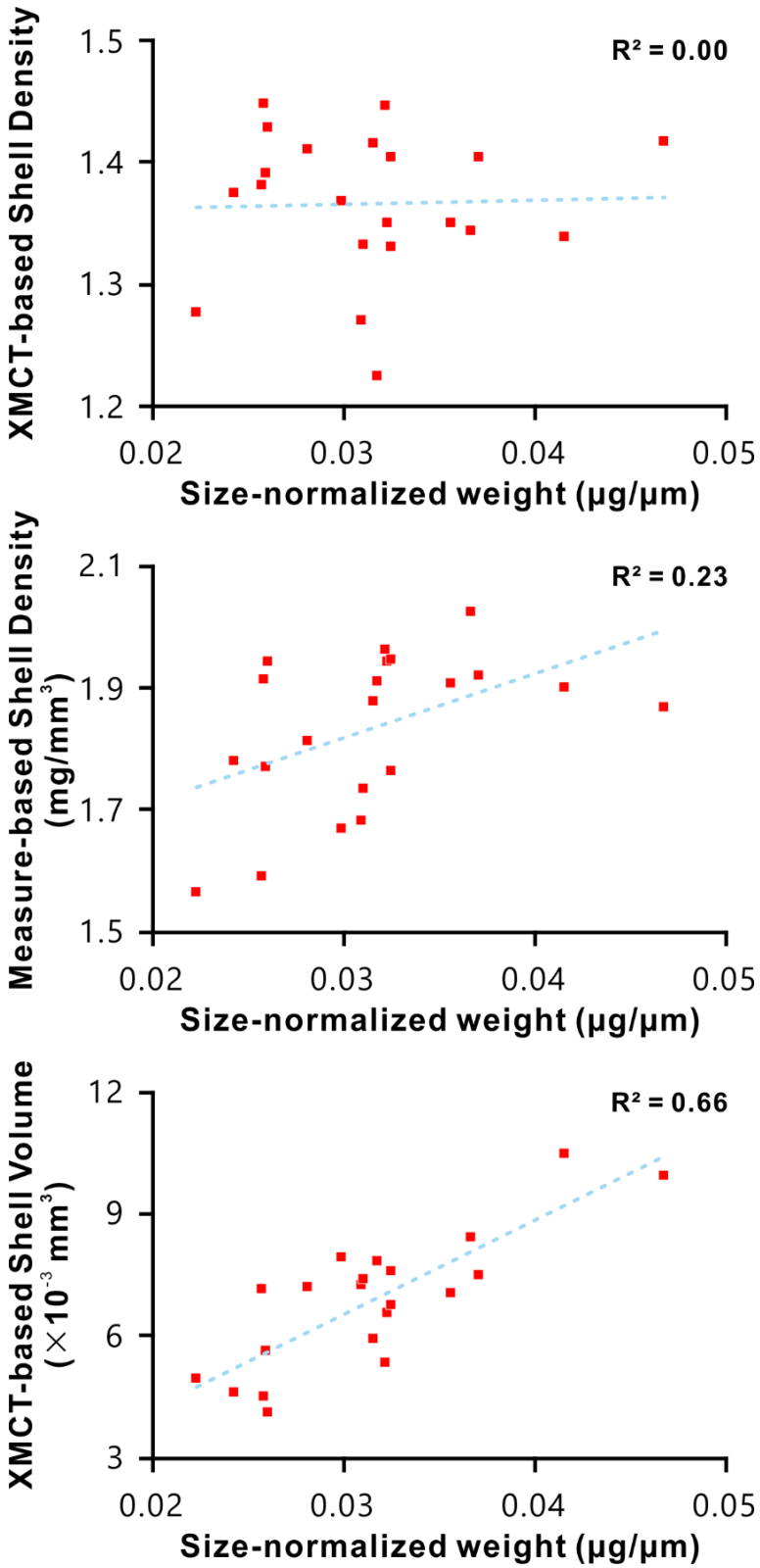

Figure 3.10 The correlation of size-normalized weight with XMCT-based shell volume and shell density.

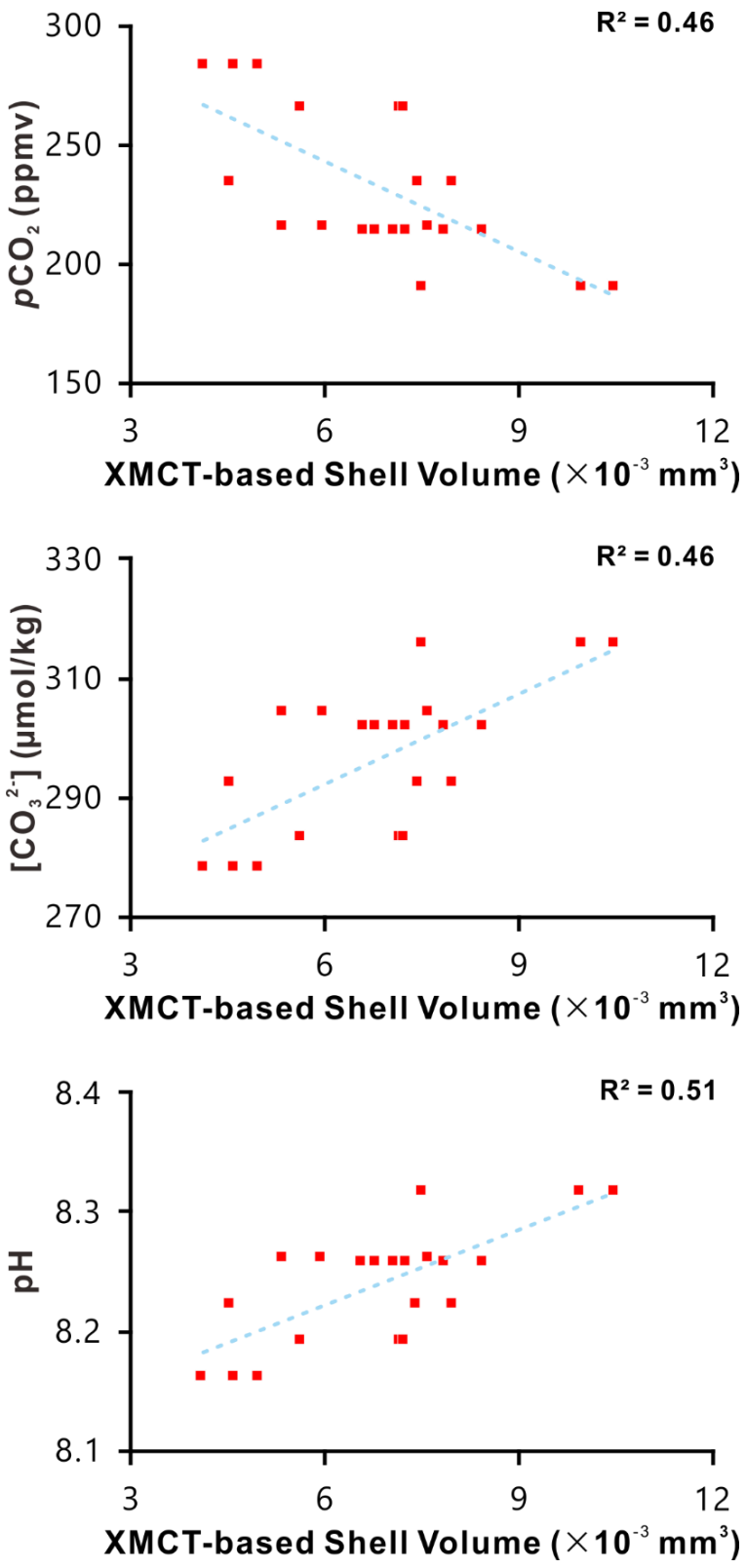

Figure 3.11 The correlation of XMCT-based shell volume and shell density with atmospheric *p*CO2, seawater [CO_3^{2-}] and pH.

5. Conclusions

The size-normalized weight measured on *G. ruber* (w) tracked the variation of atmospheric pCO_2. The result of the present study confirms the previous studies those arguing the size-normalized weight reflects surface seawater carbonate chemistry rather than SST or post-depositional alteration such as bottom water dissolution and secondary calcite precipitation. The XMCT measurement of foraminiferal shell volume and shell density improved our understanding of the representative meaning of the foraminiferal size-normalized weight. Ocean acidification affects the shell wall thickness rather than shell density of foraminiferas. This result is new direct evidence supporting previous studies. The result indicates that increasing atmospheric pCO_2 associated with ocean acidification will hinder the foraminifera to secrete thick carbonate shells, this may have a significant influence on paleoceanographic applications of the planktonic foraminiferal shell.

Chapter 4

General Summary

1. Deep-sea Fe–Mn nodules influenced by ocean acidification due to decreasing pH

With the continuous rise in atmospheric CO_2, the pH of surface seawaters will decline potentially from 8.1 to 7.4, while the pH reduction of the deep-sea counterpart will be about 0.4, declining from about 7.6 to 7.2 (Caldeira and Wickett 2003). The studies using phosphate buffer solutions and artificial seawaters revealed that elements in deep-sea Fe–Mn nodules do not simply release into seawaters according to the decreasing pH of seawaters. The element exchange across the interface between deep-sea Fe–Mn nodules and ambient seawater are controlled by sorption-desorption processes, and the element behaviors are regulated by the ion species exist in the seawaters and surface charge of the sediment surfaces. The result of the experiments by using artificial seawaters (solid-to-liquid ratio of 1/1000) shown that the release of elements those exist as cations or positively charged complexes were increased as the pH of seawater decreases. For example, the metal release of Li, Cu, Zn, and Cd will be 8 ng/g, 0.4 ng/g, 0.8 ng/g, and 0.1 ng/g, respectively, as the pH decreases from 8.1 to 7.2.

Although the seawater temperatures are different from our experiment conditions and the sediment-to-seawater ratios across the seafloor are difficult to determine, the usage of ASW and CO_2-induced pH regulation system allowed us to investigate the element behavior in response to seawater pH changes caused by ocean acidification and to estimate potential element release from deep-sea Fe–Mn nodules under the background of ocean acidification. The decreasing pH caused by ocean acidification tends to release the elements those exist as

cations or positively charged complexes into ambient seawater and restrain the release of elements those exist as inions or negatively charged complexes. This trend is not affected by temperature or sediment-to-seawater ratio. Therefore, the release of this type of elements, such as Mn, Cu, Zn and Cd, should be taken into consideration when assessing the potential influence of ocean acidification on deep-sea Fe–Mn nodules.

2. Planktonic foraminifera influenced by ocean acidification due to lowering [CO_3^{2-}]

Increasing atmospheric CO_2 promotes the dissolution of CO_2 into the oceans, hence lowers the acidity and [CO_3^{2-}] in surface seawaters. Foraminiferal individuals collected from marine sediments have completed the entire life cycle and provide a better estimate of the relationship between foraminiferal shell calcification rate and surface seawater [CO_3^{2-}]. The size-normalized weight of *G. ruber* (w) collected from the piston core MD98-2196 covaried well with the seawater pH, [CO_3^{2-}], and atmospheric pCO_2 during the past 100,000 years. The result agrees with previous studies and manifest that the size-normalized weight of planktonic foraminiferal shells reflects the carbonate chemistry of surface seawaters.

The high-resolution X-ray microcomputed tomography (XMCT) measurements provided a role to examine the post-depositional alteration on the shells and revealed the representative meaning of the size-normalized weight of foraminiferal shells. The unambiguous silhouette, clean surfaces, and well-preserved pores on the outer shells of *G. ruber* (w) tra by the high-resolution XMCT images indicate that the shells of *G. ruber* (w)

suffered from almost negligible post-depositional alteration. The good correlation between shell volume against the seawater pH, $[CO_3^{2-}]$, and atmospheric pCO_2 together with the poor correlation between shell density indicates that the changes of carbonate chemistry caused by ocean acidification affects the shell volume (i.e., shell wall thickness) rather than shell density of planktonic foraminifera *G. ruber* (w).

The result study shows that a decrease in $[CO_3^{2-}]$ caused by increasing atmospheric pCO_2 will hinder the planktonic foraminiferas to secrete thick calcite shells. A 100 ppmv increase in atmospheric pCO_2 level may lead to about 4×10^{-3} mm^3 decreases in the shell volume of *G. ruber* (w).

Reference

Aldridge, D., Beer, C. and Purdie, D. (2012). Calcification in the planktonic foraminifera *Globigerina bulloides* linked to phosphate concentrations in surface waters of the North Atlantic Ocean. Biogeosciences 9(5):1725-1739.

Archer, D. and Maier-Reimer, E. (1994). Effect of deep-sea sedimentary calcite preservation on atmospheric CO_2 concentration. Nature 367(6460):260.

Archer, D.E. (1996). An atlas of the distribution of calcium carbonate in sediments of the deep sea. Global Biogeochemical Cycles 10(1):159-174.

Awaji, S. (2009) Elucidation of the distribution and enrichment mechanism of rare metals in deep-sea mineral resources using a simple method for precise simultaneous determination of 61 elements by ICPMS. Master Dissertation, the University of Tokyo

Barker, S. and Elderfield, H. (2002). Foraminiferal calcification response to Glacial-Interglacial changes in atmospheric CO_2. Science 297(5582):833-836.

Barker, S., Kiefer, T. and Elderfield, H. (2004). Temporal changes in North Atlantic circulation constrained by planktonic foraminiferal shell weights. Paleoceanography 19(3)

Bayon, G., German, C.R., Boella, R.M., Milton, J.A., Taylor, R.N. and Nesbitt, R.W. (2002). An improved method for extracting marine sediment fractions and its application to Sr and Nd isotopic analysis. Chemical Geology 187(3):179-199.

Bé, A.W.H., Harrison, S.M. and Lott, L. (1973). *Orbulina universa* d'Orbigny in the Indian Ocean. Micropaleontology 19(2):150-192.

Beer, C.J., Schiebel, R. and Wilson, P.A. (2010). On methodologies for determining the size-normalised weight of planktic foraminifera. Biogeosciences 7(7):2193.

Beer, C.J., Schiebel, R. and Wilson, P.A. (2010). Testing planktic foraminiferal shell weight as a surface water [CO_3^{2-}] proxy using plankton net samples. Geology 38(2):103-106.

Berger, W.H. (1970). Planktonic foraminifera: selective solution and the lysocline. Marine Geology 8(2):111-138.

Bijma, J., Faber, W.W. and Hemleben, C. (1990). Temperature and salinity limits for growth and survival of some planktonic foraminifers in laboratory cultures. Journal of Foraminiferal Research 20(2):95-116.

Bijma, J., Hönisch, B. and Zeebe, R.E. (2002). Impact of the ocean carbonate chemistry on living foraminiferal shell weight: Comment on "Carbonate ion concentration in glacial-age deep waters of the Caribbean Sea" by W. S. Broecker and E. Clark. Geochemistry, Geophysics, Geosystems 3(11):1-7.

Bijma, J., Spero, H.J. and Lea, D.W. (1999). Reassessing Foraminiferal Stable Isotope Geochemistry: Impact of the Oceanic Carbonate System (Experimental Results). In: Use of Proxies in Paleoceanography: Examples from the South Atlantic. Fischer, G. and Wefer, G. (Eds.). Springer Berlin Heidelberg, Berlin, Heidelberg. 489-512.

Boehm, H.P. (1971). Acidic and basic properties of hydroxylated metal oxide surfaces. Discussions of the Faraday Society 52(0):264-275.

Broecker, W.S. and Clark, E. (2001). Glacial-to-Holocene redistribution of carbonate ion in the deep sea. Science 294(5549):2152-2155.

Broecker, W.S. and Takahashi, T. (1977). Neutralization of fossil fuel CO_2 by marine calcium carbonate. In: The fate of fossil fuel CO_2 in the oceans. Andersen, N.R. and Malahoff, A. (Eds.). Plenum Press, New York, USA. 213-242.

Brovkin, V., et al. (2002). Carbon cycle, vegetation, and climate dynamics in the Holocene: Experiments with the CLIMBER-2 model. Global Biogeochemical Cycles 16(4):86.

Brown, S.J. and Elderfield, H. (1996). Variations in Mg/Ca and Sr/Ca ratios of planktonic foraminifera caused by postdepositional dissolution: Evidence of shallow Mg-dependent dissolution. Paleoceanography 11(5):543-551.

Byrne, R.H. (2002). Inorganic speciation of dissolved elements in seawater: the influence of pH on concentration ratios. Geochemical Transactions 2(2):11-16.

Caldeira, K. and Wickett, M.E. (2003). Anthropogenic carbon and ocean pH. Nature 425(6956):365-365.

Caldeira, K. and Wickett, M.E. (2005). Ocean model predictions of chemistry changes from carbon dioxide emissions to the atmosphere and ocean. Journal of Geophysical Research 110(C9):C09S04.

Charewicz, W.A., Chaoyin, Z. and Chmielewski, T. (2001). The leaching behavior of ocean polymetallic nodules in chloride solutions. Physicochemical Problems of Mineral Processing 35:55-66.

de Moel, H., et al. (2009). Planktic foraminiferal shell thinning in the Arabian Sea due to anthropogenic ocean acidification?

De Orte, M.R., et al. (2014). Metal mobility and toxicity to microalgae associated with acidification of sediments: CO_2 and acid comparison. Marine Environmental Research 96:136-144.

de Vernal, A., Bilodeau, G., Hillaire-Marcel, C. and Kassou, N. (1992). Quantitative assessment of carbonate dissolution in marine sediments from foraminifer linings vs. shell ratios: Davis Strait, northwest North Atlantic. Geology 20(6):527-530.

de Villiers, S. (2004). Optimum growth conditions as opposed to calcite saturation as a control on the calcification rate and shell-weight of marine foraminifera. Marine Biology 144(1):45-49.

Dickson, A.G. (1990). Thermodynamics of the dissociation of boric acid in synthetic seawater from 273.15 to 318.15 K. Deep Sea Research Part A. Oceanographic Research Papers 37(5):755-766.

Dickson, A.G., Sabine, C.L. and Christian, J.R. (2007). Determination of the pH of sea water using a glass/reference electrode cell. In: Guide to best practices for ocean CO_2measurements. (Eds.). North Pacific Marine Science Organization,

Doney, S.C., Fabry, V.J., Feely, R.A. and Kleypas, J.A. (2009). Ocean Acidification: The other CO_2 problem. Annual Review of Marine Science 1(1):169-192.

Doney, S.C. and Schimel, D.S. (2007). Carbon and climate system coupling on timescales from the Precambrian to the Anthropocene. Annual Review of Environment and Resources 32:31-66.

European Communities (EC) (1998) Council Directive 98/83/EC of 3 November 1998 on the quality of water intended for human consumption. http://ec.europa.eu/environment/water/water-drink/legislation_en.html. Accessed: 2018-10-29

Endrizzi, F. and Rao, L. (2014). Chemical Speciation of Uranium(VI) in Marine Environments: Complexation of Calcium and Magnesium Ions with $[(UO_2)(CO_3)_3]^{4-}$ and the Effect on the Extraction of Uranium from Seawater. Chemistry – A European Journal 20(44):14499-14506.

Falkowski, P., et al. (2000). The Global Carbon Cycle: A Test of Our Knowledge of Earth as a System. Science 290(5490):291-296.

Feely, R.A., Orr, J., Fabry, V.J., Kleypas, J.A., Sabine, C.L. and Langdon, C. (2013). Present and future changes in seawater chemistry due to ocean acidification. In: Carbon Sequestration and Its Role in the Global Carbon Cycle. Mcpherson, B.J. and Sundquist, E.T. (Eds.). American Geophysical Union, 175-188.

Feely, R.A., et al. (2004). Impact of Anthropogenic CO_2 on the $CaCO_3$ System in the Oceans. Science 305(5682):362-366.

Field, C.B., Behrenfeld, M.J., Randerson, J.T. and Falkowski, P. (1998). Primary production of the biosphere: integrating terrestrial and oceanic components. Science 281(5374):237-240.

Foster, G.L. (2008). Seawater pH, pCO_2 and [CO^{2-}_3] variations in the Caribbean Sea over the last 130 kyr: A boron isotope and B/Ca study of planktic foraminifera. Earth and Planetary Science Letters 271(1):254-266.

Gibbs, S.J., Stoll, H.M., Bown, P.R. and Bralower, T.J. (2010). Ocean acidification and surface water carbonate production across the Paleocene–Eocene thermal maximum. Earth and Planetary Science Letters 295(3-4):583-592.

Glasby, G.P. (1991). Mineralogy, geochemistry, and origin of Pacific red clays: A review. New Zealand Journal of Geology and Geophysics 34(2):167-176.

Glasby, G.P. (2006). Manganese: Predominant Role of Nodules and Crusts. In: Marine Geochemistry. Schulz, H. and Zabel, M. (Eds.). Springer Berlin Heidelberg, 371-427.

Gonzalez-Mora, B., Sierro, F.J. and Flores, J.A. (2008). Controls of shell calcification in planktonic foraminifers. Quaternary Science Reviews 27(9):956-961.

Görög, Á., Szinger, B., Tóth, E. and Viszkok, J. (2012). Methodology of the micro-computer tomography on foraminifera. Palaeontologia Electronica 15(1):15.

Grotti, M. and Frache, R. (2007). Direct determination of arsenic in sea-water by reaction cell inductively coupled plasma mass spectrometry. Journal of Analytical Atomic Spectrometry 22(12):1481-1487.

Gupta, L.P., Kawahata, H., Takeuchi, M., Ohta, H. and Ono, Y. (2005). Temperature and pH Dependence of Some Metals Leaching from Fly Ash of Municipal Solid Waste. Resource Geology 55(4):357-372.

Hebbeln, D., Wefer, G. and Berger, W.H. (1990). Pleistocene dissolution fluctuations from apparent depth of deposition in core ERDC-127P, west-equatorial Pacific. Marine Geology 92(3-4):165-176.

Hein, J.R., Mizell, K., Koschinsky, A. and Conrad, T.A. (2013). Deep-ocean mineral deposits as a source of critical metals for high- and green-technology applications: Comparison with land-based resources. Ore Geology Reviews 51(0):1-14.

Hemleben, C., Spindler, M. and Anderson, O.R. (2012). Modern planktonic foraminifera. Springer

Ilyina, T. and Zeebe, R.E. (2012). Detection and projection of carbonate dissolution in the water column and deep-sea sediments due to ocean acidification. Geophysical Research Letters 39(6):L06606.

IPCC (2013). The fifth assessment report of the Intergovernmental Panel on Climate Change. Cambridge University Press: New York, USA

International Seabed Authority (ISA) (2018) Deep seabed minerals contractors. https://www.isa.org.jm/deep-seabed-minerals-contractors. Accessed: 2018-10-01

Iwasaki, S., Kimoto, K., Sasaki, O., Kano, H., Honda, M.C. and Okazaki, Y. (2015). Observation of the dissolution process of Globigerina bulloides tests (planktic foraminifera) by X-ray microcomputed tomography. Paleoceanography 30(4):317-331.

Iwasaki, S., et al. (2018). Effect of seawater turbulence on formation of coral primary polyp skeletons. Coral Reefs 37(3):939-944.

Johnstone, H.J.H., Schulz, M., Barker, S. and Elderfield, H. (2010). Inside story: An X-ray computed tomography method for assessing dissolution in the tests of planktonic foraminifera. Marine Micropaleontology 77(1):58-70.

Kanungo, S.B. and Das, R.P. (1988). Extraction of metals from manganese nodules of the Indian Ocean by leaching in aqueous solution of sulphur dioxide. Hydrometallurgy 20(2):135-146.

Kawahata, H., Nomura, R., Matsumoto, K. and Nishi, H. (2015). Linkage of deep sea rapid acidification process and extinction of benthic foraminifera in the deep sea at the Paleocene/Eocene transition. Island Arc 24(3):301-316.

Kester, D.R., Duedall, I.W., Connors, D.N. and Pytkowicz, R.M. (1967). Preparation of artificial seawater. Limnology and Oceanography 12(1):176-179.

Key, R.M., et al. (2004). A global ocean carbon climatology: Results from Global Data Analysis Project (GLODAP). Global Biogeochemical Cycles 18(4)

Kim, H.J., et al. (2013). Evaluation of Resuspended Sediments to Sinking Particles by Benthic Disturbance in the Clarion-Clipperton Nodule Fields. Marine Georesources & Geotechnology 33(2):160-166.

Kleypas, J.A., Buddemeier, R.W., Archer, D., Gattuso, J.-P., Langdon, C. and Opdyke, B.N. (1999). Geochemical consequences of increased atmospheric carbon dioxide on coral reefs. Science 284(5411):118-120.

Kontakiotis, G., et al. (2017). Morphological recognition of Globigerinoides ruber morphotypes and their susceptibility to diagenetic alteration in the eastern Mediterranean Sea. Journal of Marine Systems 174:12-24.

Koschinsky, A. and Halbach, P. (1995). Sequential leaching of marine ferromanganese precipitates: Genetic implications. Geochimica et Cosmochimica Acta 59(24):5113-5132.

Koschinsky, A. and Hein, J.R. (2003). Uptake of elements from seawater by ferromanganese crusts: solid-phase associations and seawater speciation. Marine Geology 198(3):331-351.

Kump, L.R., Bralower, T.J. and Ridgwell, A. (2009). Ocean acidification in deep time. Oceanography 22(4):94-107.

Langer, M.R. (2008). Assessing the contribution of foraminiferan protists to global ocean carbonate production. Journal of Eukaryotic Microbiology 55(3):163-169.

Le, J. and Shackleton, N.J. (1992). Carbonate dissolution fluctuations in the western equatorial Pacific during the late Quaternary. Paleoceanography and Paleoclimatology 7(1):21-42.

Leonhard, P., Pepelnik, R., Prange, A., Yamada, N. and Yamada, T. (2002). Analysis of diluted sea-water at the ng L^{-1} level using an ICP-MS with an octopole reaction cell. Journal of Analytical Atomic Spectrometry 17(3):189-196.

Lisiecki, L.E. and Raymo, M.E. (2005). A Pliocene-Pleistocene stack of 57 globally distributed benthic $\delta^{18}O$ records. Paleoceanography 20(1)

Lohmann, G.P. (1995). A model for variation in the chemistry of planktonic foraminifera due to secondary calcification and selective dissolution. Paleoceanography 10(3):445-457.

Lombard, F., da Rocha, R.E., Bijma, J. and Gattuso, J.P. (2010). Effect of carbonate ion concentration and irradiance on calcification in planktonic foraminifera. Biogeosciences 7(1):247-255.

Lombard, F., Labeyrie, L., Michel, E., Spero, H.J. and Lea, D.W. (2009). Modelling the temperature dependent growth rates of planktic foraminifera. Marine Micropaleontology 70(1):1-7.

Manno, C., Morata, N. and Bellerby, R. (2012). Effect of ocean acidification and temperature increase on the planktonic foraminifer *Neogloboquadrina pachyderma* (sinistral). Polar Biology 35(9):1311-1319.

Marshall, B.J., Thunell, R.C., Henehan, M.J., Astor, Y. and Wejnert, K.E. (2013). Planktonic foraminiferal area density as a proxy for carbonate ion concentration: A calibration study using the Cariaco Basin ocean time series. Paleoceanography 28(2):363-376.

Marshall, B.J., Thunell, R.C., Spero, H.J., Henehan, M.J., Lorenzoni, L. and Astor, Y. (2015). Morphometric and stable isotopic differentiation of *Orbulina universa* morphotypes from the Cariaco Basin, Venezuela. Marine Micropaleontology 120:46-64.

Martin, W.R. and Sayles, F.L. (1996). $CaCO_3$ dissolution in sediments of the Ceara Rise, western equatorial Atlantic. Geochimica et Cosmochimica Acta 60(2):243-263.

McCurdy, E. and Woods, G. (2004). The application of collision/reaction cell inductively coupled plasma mass spectrometry to multi-element analysis in variable sample matrices, using He as a non-reactive cell gas. Journal of Analytical Atomic Spectrometry 19(5):607-615.

Mekik, F. and François, R. (2006). Tracing deep-sea calcite dissolution: Agreement between the Globorotalia menardii fragmentation index and elemental ratios (Mg/Ca and Mg/Sr) in planktonic foraminifers. Paleoceanography 21(4)

Mekik, F. and Raterink, L. (2008). Effects of surface ocean conditions on deep-sea calcite dissolution proxies in the tropical Pacific. Paleoceanography and Paleoclimatology 23(1):

Metzler, C.V., Wenkam, C.R. and Berger, W.H. (1982). Dissolution of foraminifera in the eastern equatorial Pacific; an in situ experiment. The Journal of Foraminiferal Research 12(4):362-368.

Millero, F.J. (2013). Chemical Oceanography. CRC press, New York

Millero, F.J., et al. (2002). Dissociation constants for carbonic acid determined from field measurements. Deep Sea Research Part I: Oceanographic Research Papers 49(10):1705-1723.

Millero, F.J., Woosley, R., Ditrolio, B. and Waters, J. (2009). Effect of ocean acidification on the speciationof metals in seawater. Oceanography 22(4):72.

Milliman, J.D. and Droxler, A.W. (1996). Neritic and pelagic carbonate sedimentation in the marine environment: ignorance is not bliss. Geologische Rundschau 85(3):496-504.

Milliman, J.D., Troy, P.J., Balch, W.M., Adams, A.K., Li, Y.H. and Mackenzie, F.T. (1999). Biologically mediated dissolution of calcium carbonate above the chemical lysocline? Deep Sea Research Part I: Oceanographic Research Papers 46(10):1653-1669.

Moy, A.D., Howard, W.R., Bray, S.G. and Trull, T.W. (2009). Reduced calcification in modern Southern Ocean planktonic foraminifera. Nature Geoscience 2:276-280.

Naik, S.S. and Naidu, P.D. (2007). Calcite dissolution along a transect in the western tropical Indian Ocean: A multiproxy approach. Geochemistry, Geophysics, Geosystems 8(8)

Naik, S.S., Naidu, P.D., Govil, P. and Godad, S. (2010). Relationship between weights of planktonic foraminifer shell and surface water $CO_3^{=}$ concentration during the Holocene and Last Glacial Period. Marine Geology 275(1):278-282.

National Oceanic and Atmospheric Administration (NOAA) (2018) Trends in atmospheric carbon dioxide. https://www.esrl.noaa.gov/gmd/ccgg/trends/gl_full.html.

Oebius, H.U., Becker, H.J., Rolinski, S. and Jankowski, J.A. (2001). Parametrization and evaluation of marine environmental impacts produced by deep-sea manganese nodule mining. Deep Sea Research Part II: Topical Studies in Oceanography 48(17–18):3453-3467.

Orr, J.C., et al. (2005). Anthropogenic ocean acidification over the twenty-first century and its impact on calcifying organisms. Nature 437(7059):681-686.

Osborne, E.B., et al. (2016). Calcification of the planktonic foraminifera Globigerina bulloides and carbonate ion concentration: Results from the Santa Barbara Basin. Paleoceanography 31(8):1083-1102.

Pälike, H., et al. (2012). A Cenozoic record of the equatorial Pacific carbonate compensation depth. Nature 488:609-615.

Parida, K., Satapathy, P.K. and Das, N. (1996). Studies on Indian Ocean Manganese Nodules: IV. Adsorption of Some Bivalent Heavy Metal Ions onto Ferromanganese Nodules. Journal of Colloid and Interface Science 181(2):456-462.

Park, K. (1966). Deep-Sea pH. Science 154(3756):1540-1542.

Peterson, M.N.A. (1966). Calcite: Rates of dissolution in a vertical profile in the Central Pacific. Science 154(3756):1542-1544.

Petit, J.-R., et al. (1999). Climate and atmospheric history of the past 420,000 years from the Vostok ice core, Antarctica. Nature 399(6735):429-436.

Raven, J., et al. (2005). Ocean acidification due to increasing atmospheric carbon dioxide. The Royal Society

Reimer, P.J., et al. (2013). IntCal13 and Marine13 Radiocarbon Age Calibration Curves 0–50,000 Years cal BP. Radiocarbon 55(4):1869-1887.

Ridgwell, A. and Zeebe, R.E. (2005). The role of the global carbonate cycle in the regulation and evolution of the Earth system. Earth and Planetary Science Letters 234(3-4):299-315.

Riebesell, U., Zondervan, I., Rost, B., Tortell, P.D., Zeebe, R.E. and Morel, F.M.M. (2000). Reduced calcification of marine plankton in response to increased atmospheric CO_2. Nature 407:364-367.

Roy, R.N., et al. (1993). The dissociation constants of carbonic acid in seawater at salinities 5 to 45 and temperatures 0 to 45°C. Marine Chemistry 44(2):249-267.

Russell, A.D., Hönisch, B., Spero, H.J. and Lea, D.W. (2004). Effects of seawater carbonate ion concentration and temperature on shell U, Mg, and Sr in cultured planktonic foraminifera. Geochimica et Cosmochimica Acta 68(21):4347-4361.

Sabine, C.L., et al. (2004). The oceanic sink for anthropogenic CO_2. Science 305(5682):367-371.

Schiebel, R. (2002). Planktic foraminiferal sedimentation and the marine calcite budget. Global Biogeochemical Cycles 16(4):3-1-3-21.

Schiebel, R. and Hemleben, C. (2017). Planktic foraminifers in the modern ocean. Springer,

Schindler, P.W. (1975). Removal of trace metals from the oceans: a zero order model. Thalassia Jugosl. 11:101-111.

Schmidt, D.N., Renaud, S., Bollmann, J., Schiebel, R. and Thierstein, H.R. (2004). Size distribution of Holocene planktic foraminifer assemblages: biogeography, ecology and adaptation. Marine Micropaleontology 50(3):319-338.

Senanayake, G. (2011). Acid leaching of metals from deep-sea manganese nodules – A critical review of fundamentals and applications. Minerals Engineering 24(13):1379-1396.

Sharma, R. (2015). Environmental Issues of Deep-Sea Mining. Procedia Earth and Planetary Science 11:204-211.

Spero, H.J., Bijma, J., Lea, D.W. and Bemis, B.E. (1997). Effect of seawater carbonate concentration on foraminiferal carbon and oxygen isotopes. Nature 390:497-500.

Stumm, W., Huang, C.P. and Jenkins, S.R. (1970). Specific chemical interaction affecting stability of dispersed systems. Croatica Chemica Acta 42(2):223-245.

Stumm, W. and Morgan, J.J. (1996). Aquatic Chemistry, 3rd ed. Wiley, New York.

Terashima, S., Imai, N., Taniguchi, M., Okai, T. and Nishimura, A. (2002). The Preparation and Preliminary Characterisation of Four New Geological Survey of Japan Geochemical Reference Materials: Soils, JSO-1 and JSO-2; and Marine Sediments, JMS-1 and JMS-2. Geostandards Newsletter 26(1):85-94.

Terashima, S., Usui, A. and Imai, N. (1995). Two new GSJ geochemical reference samples: syenite Jsy-1 and manganese nodule JMn-1. Geostandards Newsletter 19(2):221-229.

Tessier, A., Campbell, P.G.C. and Bisson, M. (1979). Sequential extraction procedure for the speciation of particulate trace metals. Analytical Chemistry 51(7):844-851.

Ujiié, Y. and Ujiié, H. (2006). Dynamic changes of the surface and intermediate waters in the Ryukyu Arc region during the past ~250,000 years: based on planktonic and benthic foraminiferal analyses of two IMAGES cores. Fossils 79:43-59.

Ujiié, Y., Asahi, H., Sagawa, T. and Bassinot, F. (2016). Evolution of the North Pacific Subtropical Gyre during the past 190 kyr through the interaction of the Kuroshio Current with the surface and intermediate waters. Paleoceanography 31(11):1498-1513.

United States Environmental Protection Agency (USEPA) (2018) 2018 Drinking Water Standards and Advisory Tables. https://www.epa.gov/dwstandardsregulations/2018-drinking-water-standards-and-advisory-tables.

Verlaan, P.A., Cronan, D.S. and Morgan, C.L. (2004). A comparative analysis of compositional variations in and between marine ferromanganese nodules and crusts in the South Pacific and their environmental controls. Progress in Oceanography 63(3):125-158.

Wang, Q., Kawahata, H., Manaka, T., Yamaoka, K. and Suzuki, A. (2017). Potential Influence of Ocean Acidification on Deep-Sea Fe–Mn Nodules: Results from Leaching Experiments. Aquatic Geochemistry 23(4):233-246.

Weinkauf, M., Moller, T., Koch, M.C. and Kucera, M. (2013). Calcification intensity in planktonic Foraminifera reflects ambient conditions irrespective of environmental stress. Biogeosciences 10(10):6639-6655.

Weinkauf, M.F., Kunze, J.G., Waniek, J.J. and Kučera, M. (2016). Seasonal variation in shell calcification of planktonic Foraminifera in the NE Atlantic reveals species-specific response to temperature, productivity, and optimum growth conditions. PLOS ONE 11(2):e0148363.

World Health Organization (WHO) (2011) Guidelines for drinking-water quality (4th Edition). http://www.who.int/water_sanitation_health/publications/2011/dwq_guidelines/en/.

Yuan-Hui, L. (1991). Distribution patterns of the elements in the ocean: A synthesis. Geochimica et Cosmochimica Acta 55(11):3223-3240.

Zaman, M.I., Mustafa, S., Khan, S. and Xing, B. (2009). Effect of phosphate complexation on Cd^{2+} sorption by manganese dioxide (β-MnO_2). Journal of Colloid and Interface Science 330(1):9-19.

Zeebe, R.E. and Wolf-Gladrow, D. (2001). CO_2 in seawater: equilibrium, kinetics, isotopes. Elsevier, New York

Acknowledgement

I firstly want to express my sincere gratefulness to my supervisor, Professor Hodaka Kawahata. I sincerely appreciate him for providing me this precious opportunity to study as a Ph.D. student at the University of Tokyo, and for his supports and advises in all aspects of the studies and researches during my Ph.D. course. I also want to express my hearty appreciation to Dr. Atsushi Suzuki in AIST for so many supports on ICP-MS operations, pH measurements, and making artificial seawater. I am grateful to Dr. Kyoko Yamaoka in AIST for her plentiful help on ICP-MS measurements and data interpretation, and I appreciate her for so many constructive discussions and valuable comments. I also thank Dr. Azumi Kuroyanagi in Tohoku University for so much kind help when I conducted XMCT data processing at Tohoku University. I appreciate her for teaching me about the planktonic foraminifera. Her advises enlightened me so much. Shunichi Kinoshita in Tohoku University also provided me many valuable suggestions and comments when I performed XMCT measurements at Kochi Core Center and when I processed XMCT data at Tohoku University. I sincerely thank Dr. Masafumi Murayama in Kochi Core Center for providing me the chance to perform XMCT measurements at his laboratory. I am grateful to Dr. Yurika Ujiié in Kochi Core Center for providing me the samples of the core MD98-2196 and the detailed information about these samples. I also thank her for the kind assistance when I sampled the core at Kochi Core Center. I appreciate Dr. Toshihiro Yoshimura (JAMSTEC), Dr. Junichiro Kuroda (the Univesity of Tokyo), Dr. Akira Usui (Kochi University) for their kind suggestions on improving the experiments, presentations, and manuscripts.

I want to appreciate Dr. Shinya Iwasaki (JAMSTEC) for advising me on planktonic foraminifera. I want to thank Dr. Yuta Isaji in JAMSTEC for his kind guidance, encouragement on writing the thesis. I also received so much encouragement from Dr. Hiroki Matsui in Kochi Core Center during the tough time in the research, and I also appreciate his advice on the pre-treatment of planktonic foraminifera. I thank Yuki Ota and (the University of Tokyo) for helping me with the hand-picking of planktonic foraminifera and the measurement on ICP-MS. I thank Dr. Takuya Manaka (Forestry and Forest Products Research Institute) for his kind tutorship when I came to Japan and also for his guidance on research when I just started my experiments. I am grateful to Ayumi Maeda for guided me concerning the pre-treatment and the hand-picking of planktonic foraminifera. I am grateful to Dr. Masayuki Nagao, Dr. Toru Tamura, and Yumiko Yoshinaga for so much kind help and assistance when I conducted leaching experiment and ICP-MS measurements at AIST.

I also would like to thank other members in Kawahata Lab, Rica Uchida, Jiwon Eom, Hiroto Kajita, Yoko Nishikura. I also thank all the members in the Department of the Ocean Floor Geosciences, Atmosphere and Ocean Research Institue, the University of Tokyo.

Finally, my sincere gratefulness to my wife, Atsuko T. Wang, for her continuous and constant supports until today. I also want to thank my parents-in-law for their goodness and encouragement. I thank my parents, my elder sister, my elder brother, whom I cannot meet often, but I know their supports and encouragements are always with me.